Supplementary Information

Light-induced in situ chemical activation of a fluorescent probe for monitoring intracellular G-quadruplex structures

Marco Deiana,[a*†] Maëlle Mosser,[b†] Tangui Le Bahers,[b] Elise Dumont,[b] Marta Dudek,[c] Sandrine Denis-Quanquin,[b] Nasim Sabouri,[a] Chantal Andraud,[b] Katarzyna Matczyszyn,[c] Cyrille Monnereau[b*] and Laure Guy[b*]

[a] Department of Medical Biochemistry and Biophysics, Umeå University, 90187 Umeå, Sweden

[b] Univ Lyon, ENS de Lyon, CNRS UMR 5182, Université Claude Bernard Lyon 1, Laboratoire de Chimie, F69342, Lyon, France

[c] Advanced Materials Engineering and Modelling Group, Faculty of Chemistry, Wroclaw University of Science and Technology, Wyb. Wyspianskiego 27, 50-370 Wroclaw, Poland

* To whom correspondence should be addressed. marco.deiana@umu.se ; cyrille.monnereau@ens-lyon.fr ; laure.guy@ens-lyon.fr

† Joint First Authors

Synthesis

All experiments were conducted under normal atmospheric conditions. Analytical thin layer chromatography was performed on glass plates coated with 0.25-mm 230-400 mesh silica gel containing a fluorescent indicator. Column chromatography was performed using silica gel (spherical neutral, particle's size of 63-210 µm). NMR spectra (^{1}H, ^{13}C) were recorded at 298 K on a Bruker Avance III 400 MHz spectrometer equipped with a Prodigy broad band probe at 400.140 MHz and 100.615 MHz, respectively. Data were listed in parts per million (ppm) and were reported relative to tetramethylsilane. Residual solvent peaks were used as internal standard.

Compound 1

Cs_2CO_3 (877 mg, 2.7 mmol) is added to a solution of the HBr, bis-phenol[59] (400 mg, 0.6 mmol) and 2,5,8,11,14-pentaoxahexadecan-16-yl 4-methylbenzensulfonate (547 mg, 1.3 mmol) in DMF (30 mL). The solution is heated at 100 °C for 15 h. DMF is evaporated and replaced by CH_2Cl_2 (50 mL). After filtration, the solution is concentrated under reduced pressure to give a crude product (550 mg), which is purified by column chromatography over silica gel eluted with a gradient of CH_2Cl_2/EtOAc from 100:0 to 60:40, giving **1** as a brown oil (423 mg, 72%).

^{1}H NMR (400.1 MHz, $CDCl_3$) δ 7.49 (dd, *J* = 7.92, 0.85 Hz, 1H), 7.42 (s, 1H), 7.38 (td, *J* = 7.49, 1.40 Hz, 1H), 7.29 (td, *J* = 8.10, 1.16 Hz, 1H), 7.23 (d, *J* = 8.10 Hz, 1H), 7.18 (d, *J* = 8.22 Hz, 1H), 7.09 (d, *J* = 8.22 Hz, 1H), 4.1 (m, 2H), 3.65-3.40 (m, 18 H), 3.39 (s, 3H), 2.73 (m, 2H), 2.54 (m, 1H), 1.95 (m, 1H); **^{13}C NMR** (100.615 MHz, $CDCl_3$) δ 157.30 (Cq), 153.84 (Cq), 146.40 (Cq), 133.50 (Cq), 133.23 (Cq), 131.94 (Cq), 131.36 (CH), 130.51 (Cq), 129.56 (CH), 127.44 (CH), 126.52 (Cq), 126.16 (CH), 126.15 (CH), 125.42 (CH), 114.65 (CH), 71.94 (CH_2), 70.58 (CH_2,), 70.57 (CH_2), 70.52 (CH_2), 70.51 (2 CH_2), 70.48 (CH_2), 70.37 (CH_2), 69.67 (CH_2), 69.54 (CH_2), 59.03 (CH_3), 29.29 (CH_2), 29.16 (CH_2); **HRMS (ESI)** $[M+2H]^{2+}$: calcd. for $C_{56}H_{68}N_2O_{12}$ 481.2459; found: 481.2449.

Compound 1'

The protonated bis-phenol is neutralized prior to use by dissolution in CH_2Cl_2 and addition of K_2CO_3. The mixture is stirred for 15 h and the resulting solid is filtered off. The solvent is removed from the filtrate to give a beige solid.

Under argon, distilled pyridine (2 mL, 24 mmol) is added to a solution of the bis phenol precursor (560 mg, 1.14 mmol) in dichloromethane (20 mL). Triflic anhydride (0.5 mL, 3 mmol) is added dropwise at 0 °C to the mixture and the solution is stirred for 15 h at room temperature. The organic layer is washed

three times with water (15 mL), once with a saturated solution of NaCl (5 mL) and dried over Na_2SO_4. The solvent is removed under reduced pressure to give a crude product (678 mg), which is purified by chromatography over silica gel eluted with CH_2Cl_2/petroleum ether 50:50, giving a beige solid (593 mg, 70 %).

^{1}H NMR (400.10 Hz, CD_3CN): δ 7.82 (s, 2H), 7.67 (dd, *J* = 1.10 Hz, 7.82 Hz, 2H), 7.61 (d, *J*= 8.52 Hz, 2H), 7.49 (s, 2H), 7.47 (m, 2H), 7.43 (m, 2H), 7.15 (d, *J* = 8.36 Hz, 2H), 3.02 (m, 4H), 2.88 (m, 2H), 2.55 (m, 2H) ; **^{13}C NMR** (100.61 MHz, CD_3CN): δ 152.53 (Cq), 148.30 (Cq), 146.58 (Cq), 141.33 (Cq), 136.10 (Cq), 133.32 (CH), 132.20 (Cq), 130.15 (Cq), 129.55 (CH), 129.29 (CH), 128.98 (CH), 127.73 (Cq), 127.30 (CH), 127.19 (CH), 121.36 (CH), 29.22 (CH_2), 28.61 ppm (CH_2) ; **^{19}F NMR** ($CDCl_3$): δ = −75.02, **HMRS (ESI)** $[M+H]^+$: calcd. for $C_{36}H_{22}F_6N_2O_6S_2$ 757.0896, found 757.0889.

Compound 2

Procedure A: 3 mL of solution of **1** in H_2O (c = 10^{-5} M) are irradiated at 350 nm in a quartz cells with the lamp of the Horiba spectrofluorometer (with excitation and emission slits opened at 350 nm and 460 nm, respectively, corresponding to an irradiation power of 2 mW) for an hour. The irradiation is run four times on four other 3 mL of solution of **1** in H_2O. All the irradiated solutions (total 12 mL) are gathered and lyophilized until 1 mL solution remains then 0.1 mL of D_2O is added for NMR analyses.

^{1}H NMR (1000.3 MHz, H_2O+D_2O10%): δ 9.27 (d, *J* = 7.91 Hz, 1H), 9.03 (s, 1H), 8.98 (d, *J* = 8.39 Hz, 1H), 8.40 (d, *J* = 7.25 Hz, 1H), 8.26 (d, *J* = 7.91 Hz, 1H), 8.11 (t, *J* = 7.22 Hz, 1H), 8.03 (t, *J* = 7.22 Hz, 1H), 3.72 (2H), 3.67 (2H) ; **^{13}C NMR** (251.53 MHz, H_2O+D_2O10%): δ = 144.74 (Cq), 143.73 (Cq), 142.71 (CH), 136.70 (Cq), 133.15 (CH), 130.29 (CH), 130.06 (CH), 129.91 (CH), 129.61 (CH), 129.60 (Cq), 129.52 (Cq), 121.93 (CH), 121.10 (Cq), 120.16 (Cq), 26.57 (CH_2), 26.09 (CH_2).**HMRS (ESI)** m/z $[M]^{2+}$ calcd. for $C_{34}H_{22}N_2$ 229.0886, found 229.0896.

Procedure B (in CH_2Cl_2): 50 mL of solution of **1**' in CH_2Cl_2 (c = 1.2 10^{-4} M) are placed in a quartz flask, stirred and irradiated at 340 nm with a LED (55mW) beam focalized on the flash using a lens. The conversion is monitored by UV absorption spectra of the reaction mixture, the irradiation is stopped after 15 hours when the conversion is optimum (monitored by UV/vis spectroscopy). To the solution CH_2Cl_2 are added 25 mL of a NaCl solution (c = 1.3 10^{-2} M) and the solution vigorously stirred in a closed flask for 12 hours. The two phases are then separated. According to the HPLC, ^{1}H and ^{13}C NMR (see figure S13-S15), the separation is efficient while the organic phase contains the unreacted **1'** and the aqueous phase contains **2** as its chloride salt without further purification.

NMR

Spectra of **1**

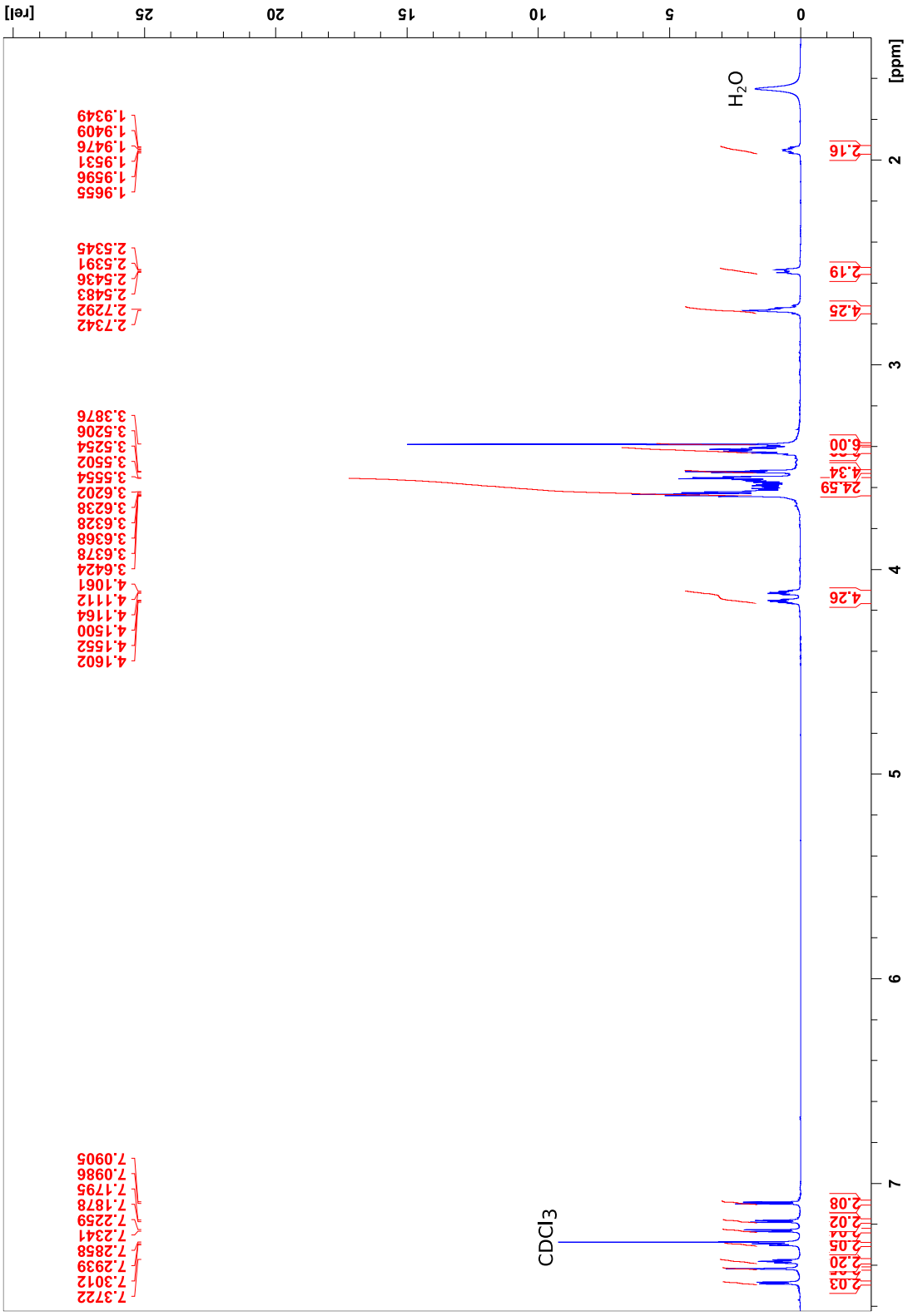

Figure S1 ^{1}H NMR ($CDCl_3$, 400.140 MHz) of **1**.

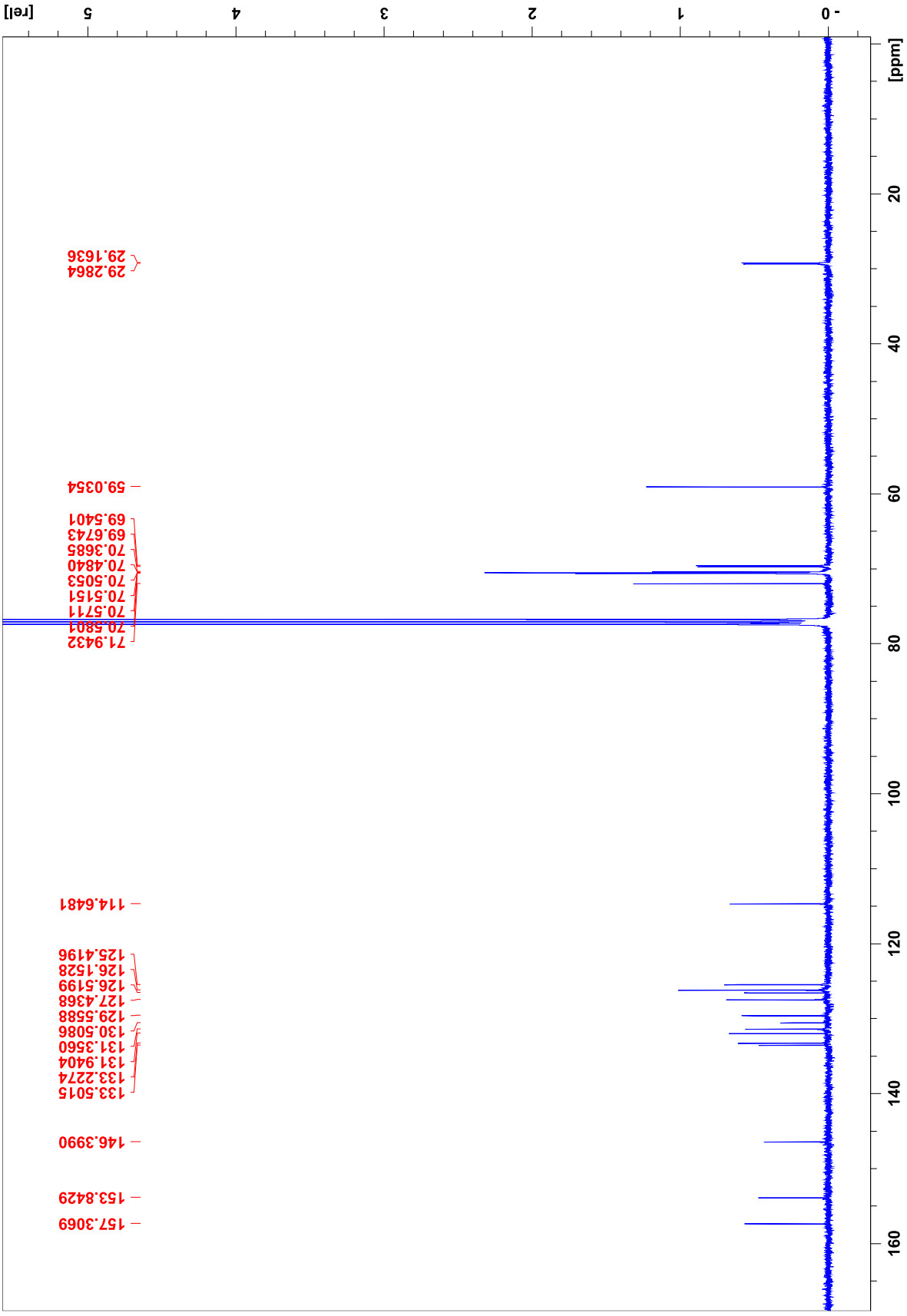

Figure S2 ^{13}C NMR ($CDCl_3$, 100.615 MHz) of **1**.

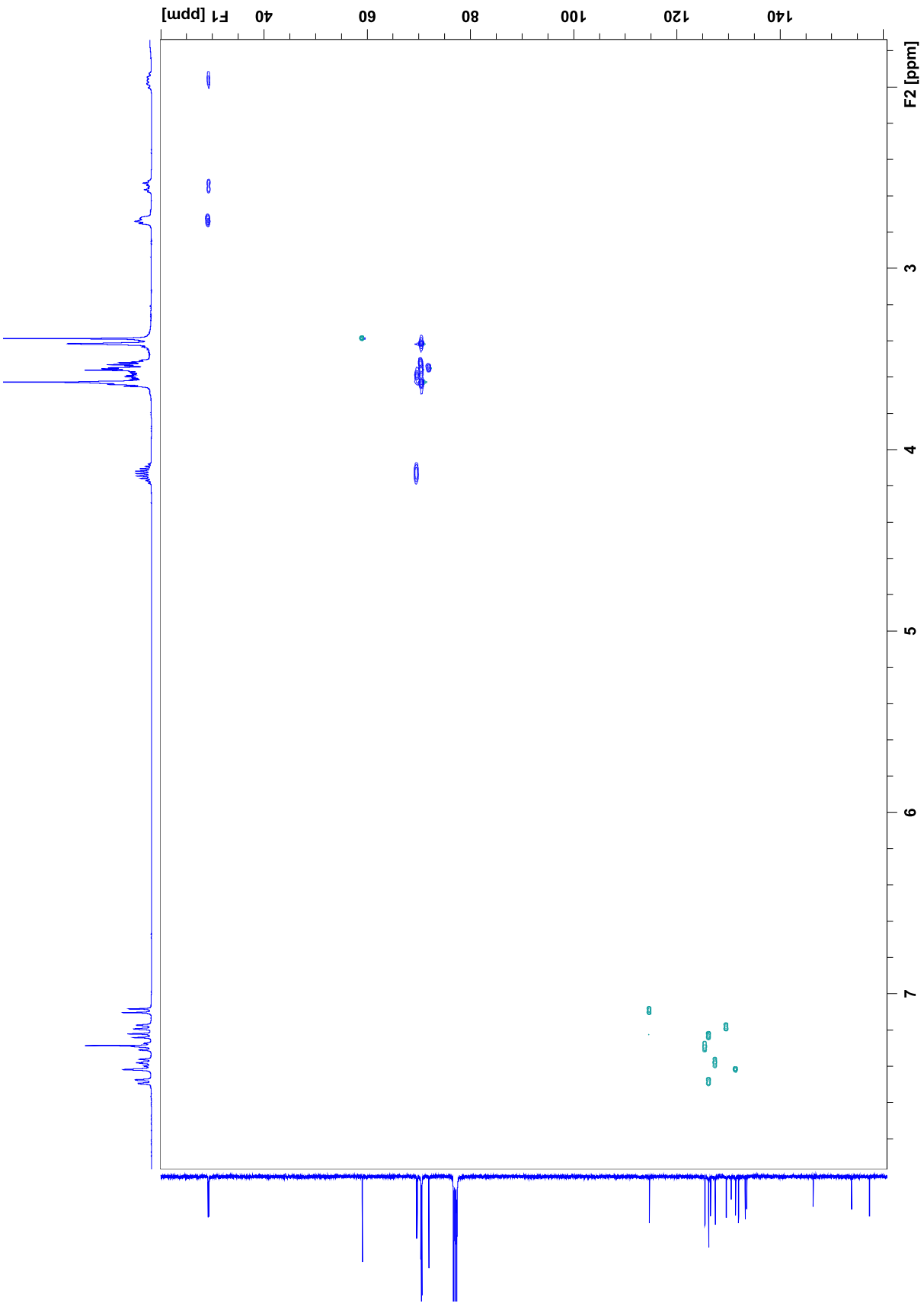

Figure S3 HSQC ($CDCl_3$, 400.140 MHz) of **1**.

Spectra of **1'**

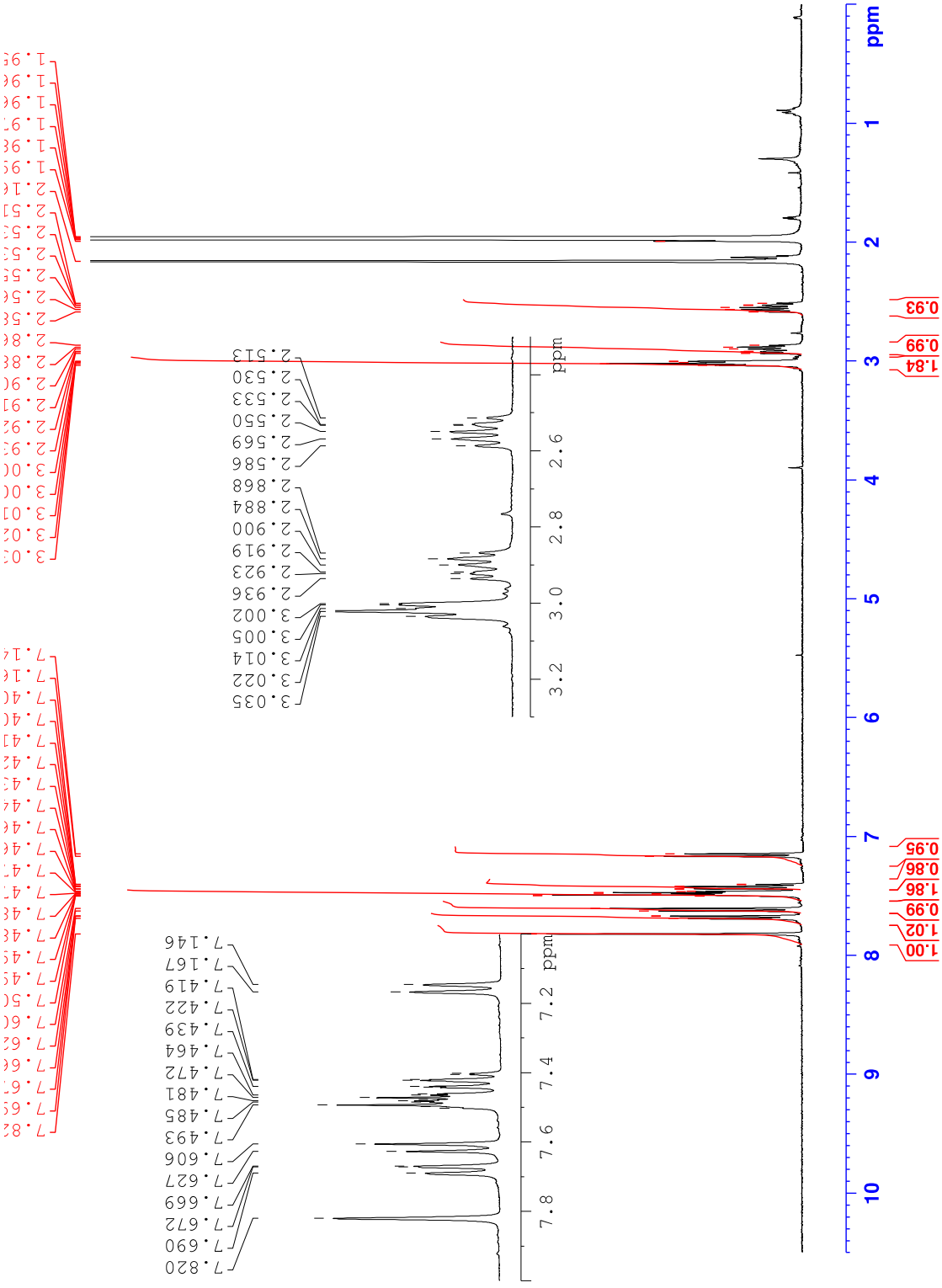

Figure S4 ^{1}H NMR (CD_3CN 400.140 MHz) of **1'**.

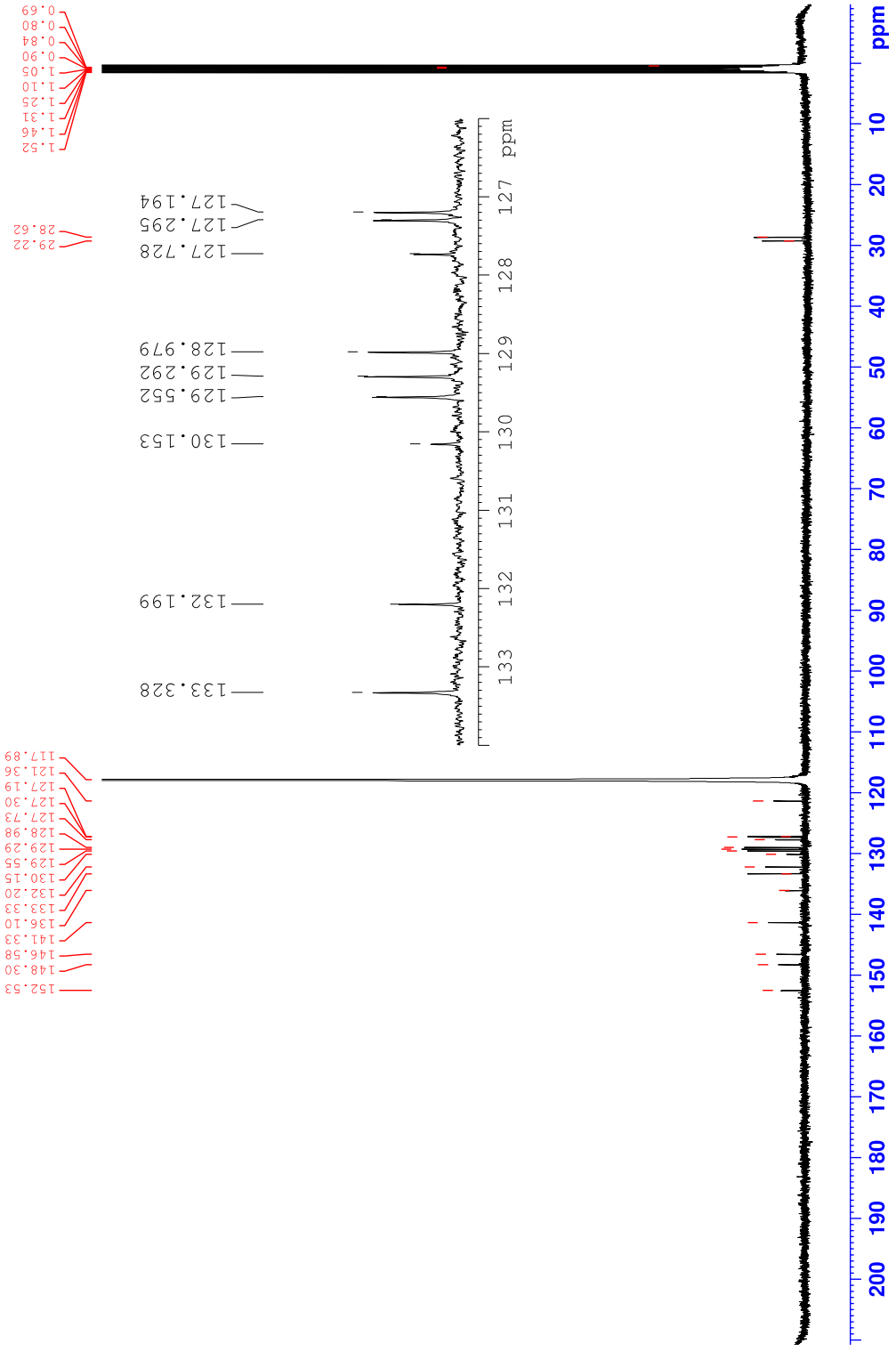

Figure S5 ^{13}C NMR (CD_3CN 100. 615 MHz) of **1'**.

Spectra of **2 (procedure A)** recorded at 1GHz for the structure elucidation

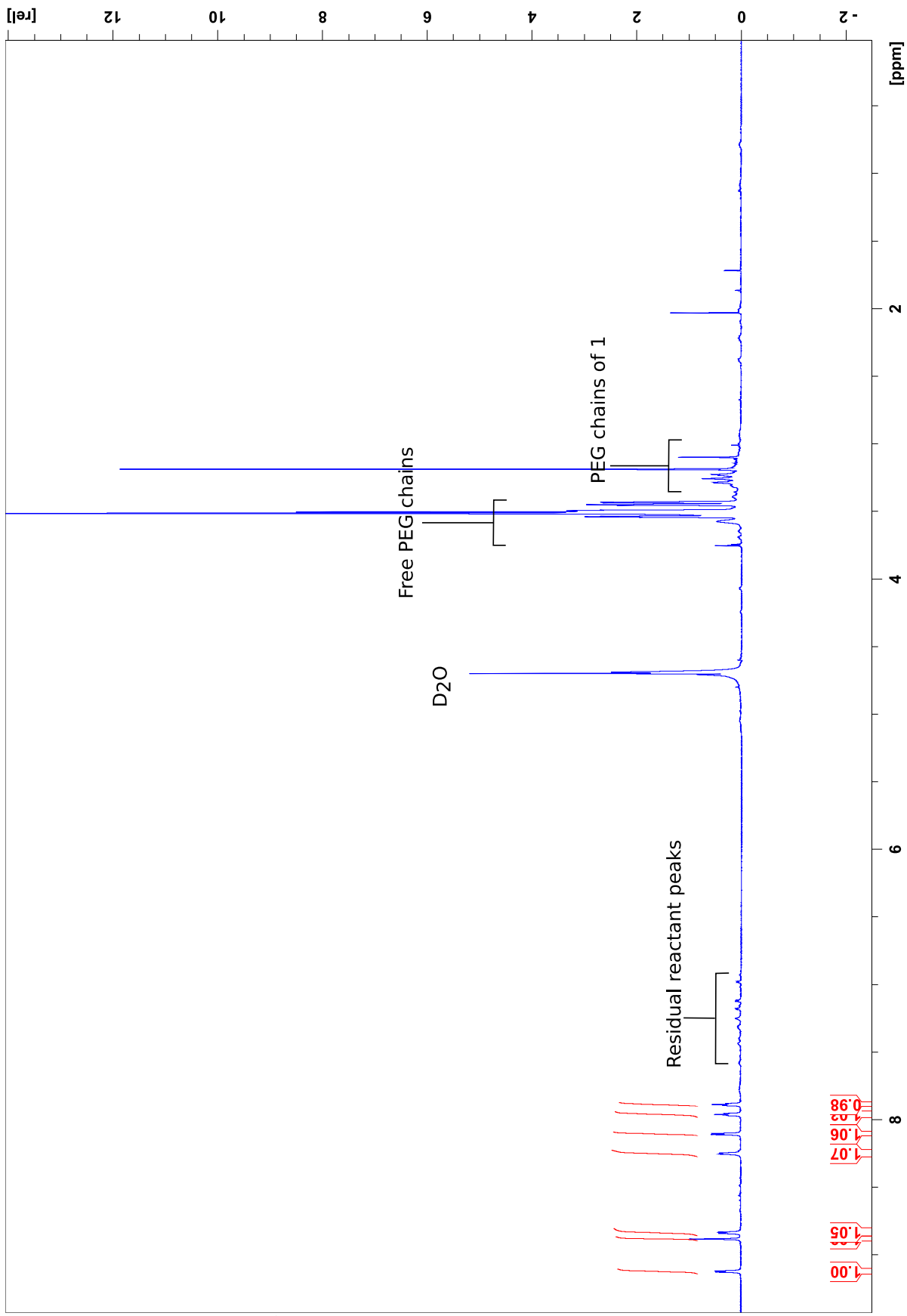

Figure S6 ^{1}H NMR (H_2O + 10% D_2O, 1000.3 MHz) of **2**.

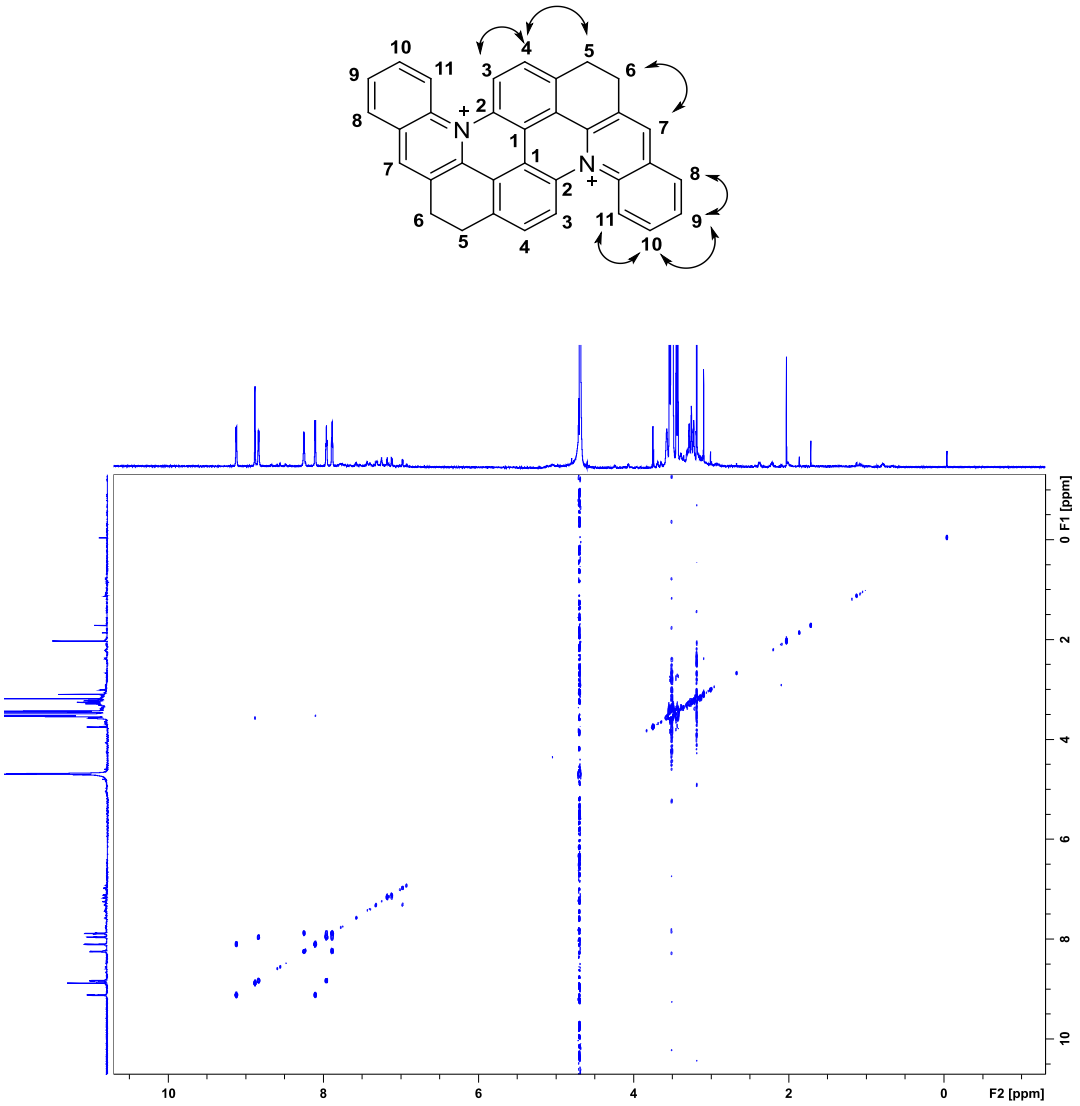

Figure S7 COSY (H_2O + 10% D_2O, 1000.3 MHz) of **2**.

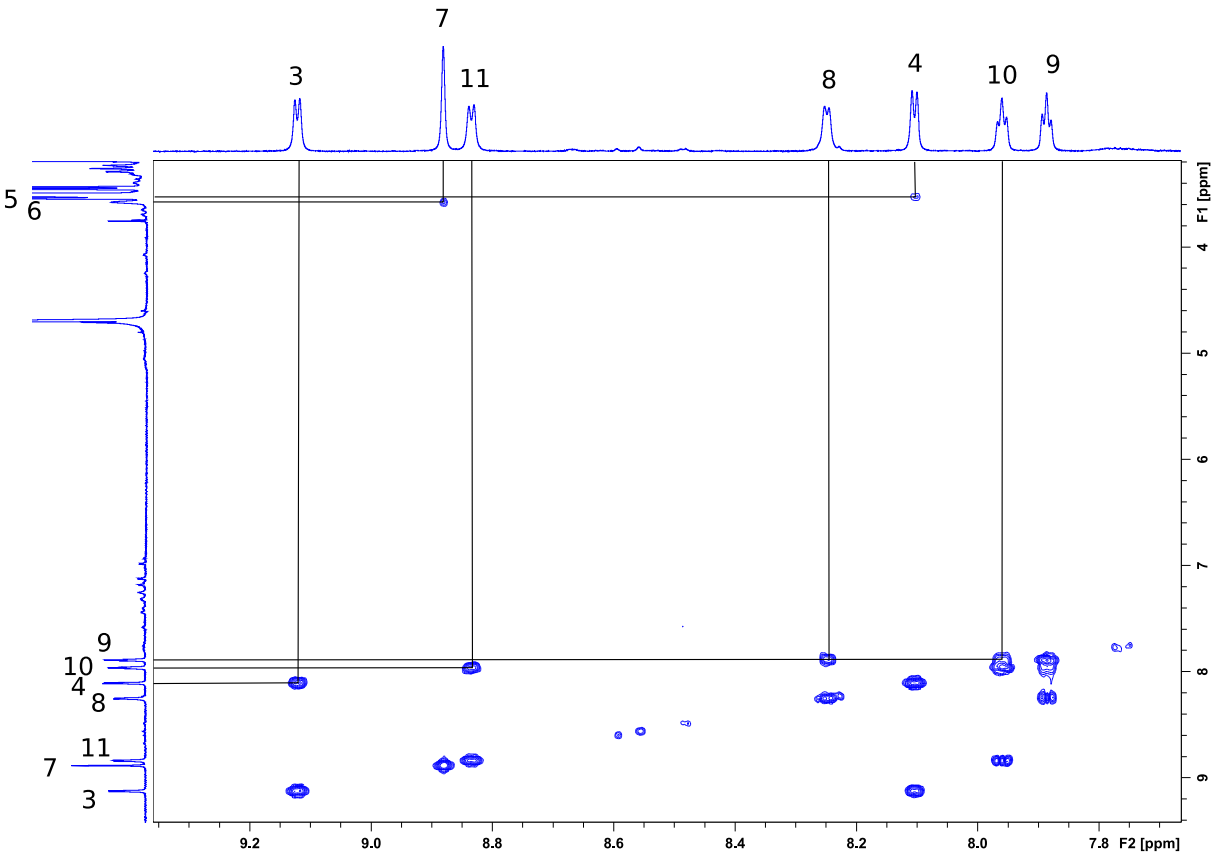

Figure S8 Expanded region of the COSY spectrum (H_2O + 10% D_2O, 1000.3 MHz) of **2**.

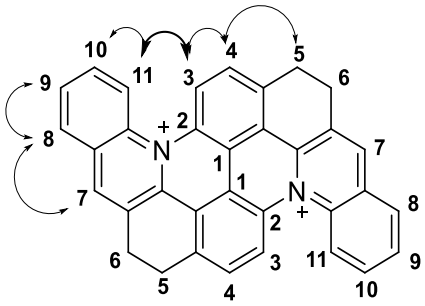

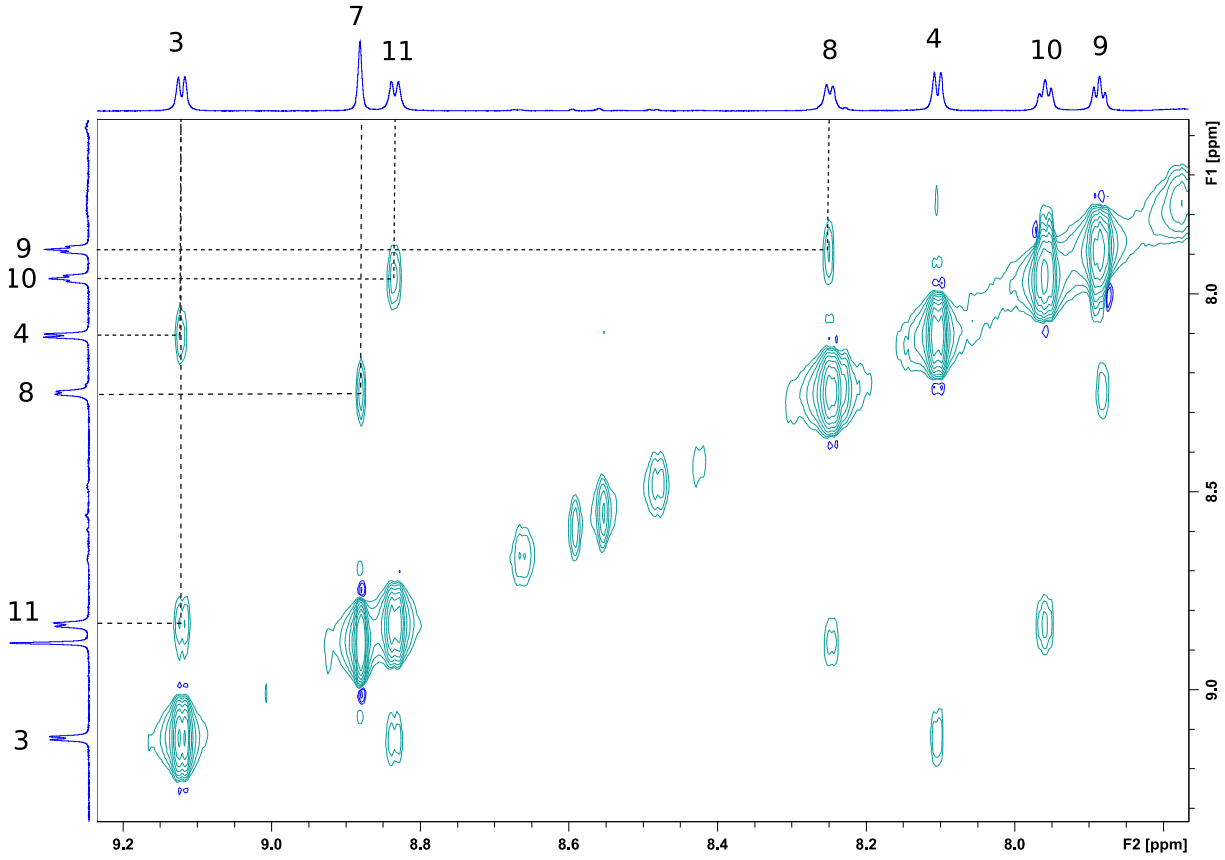

Figure S9 NOESY (H_2O + 10% D_2O, 1000.3 MHz) of **2**.

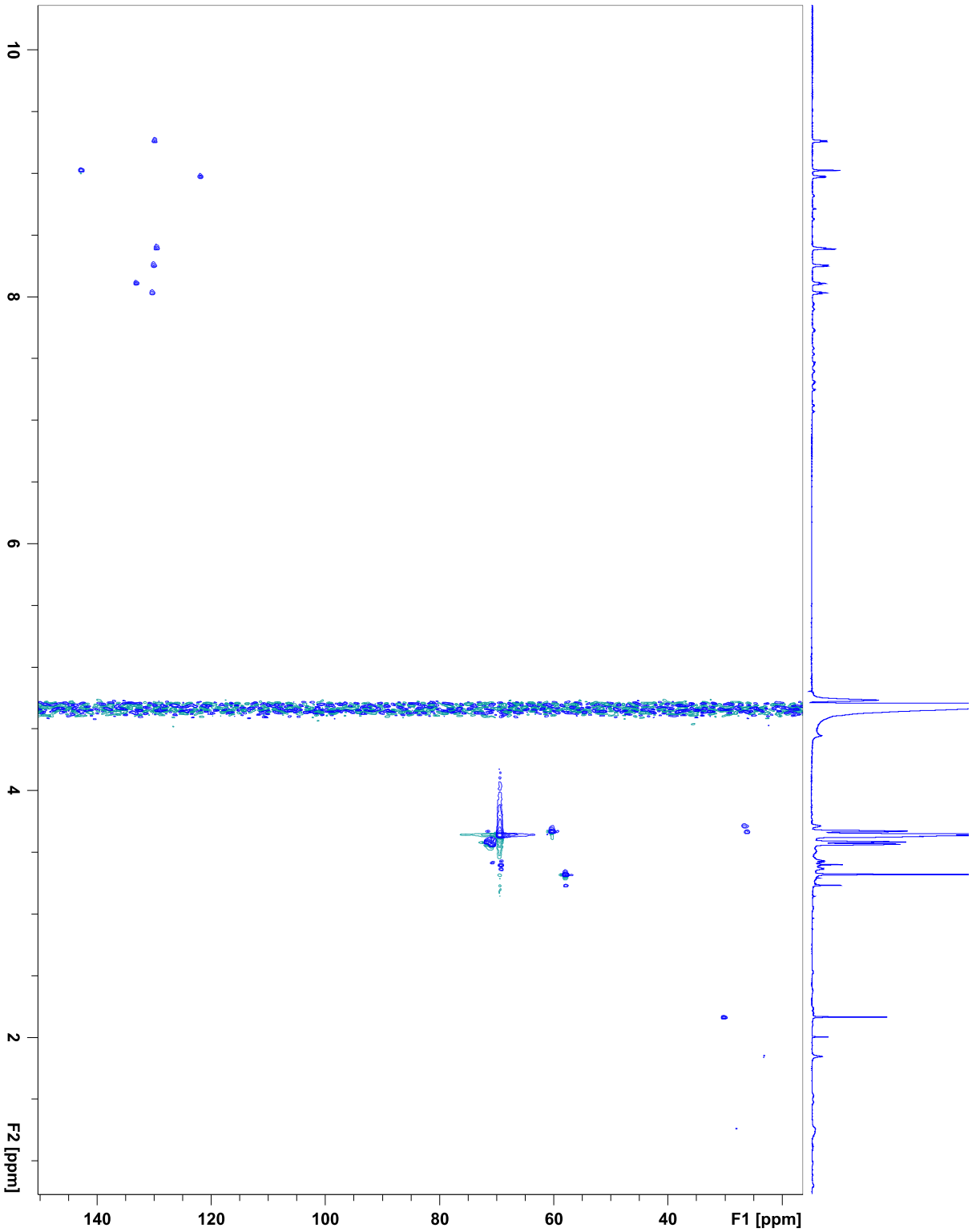

Figure S10 HSQC (H_2O + 10% D_2O, 1000.3 MHz) of **2**.

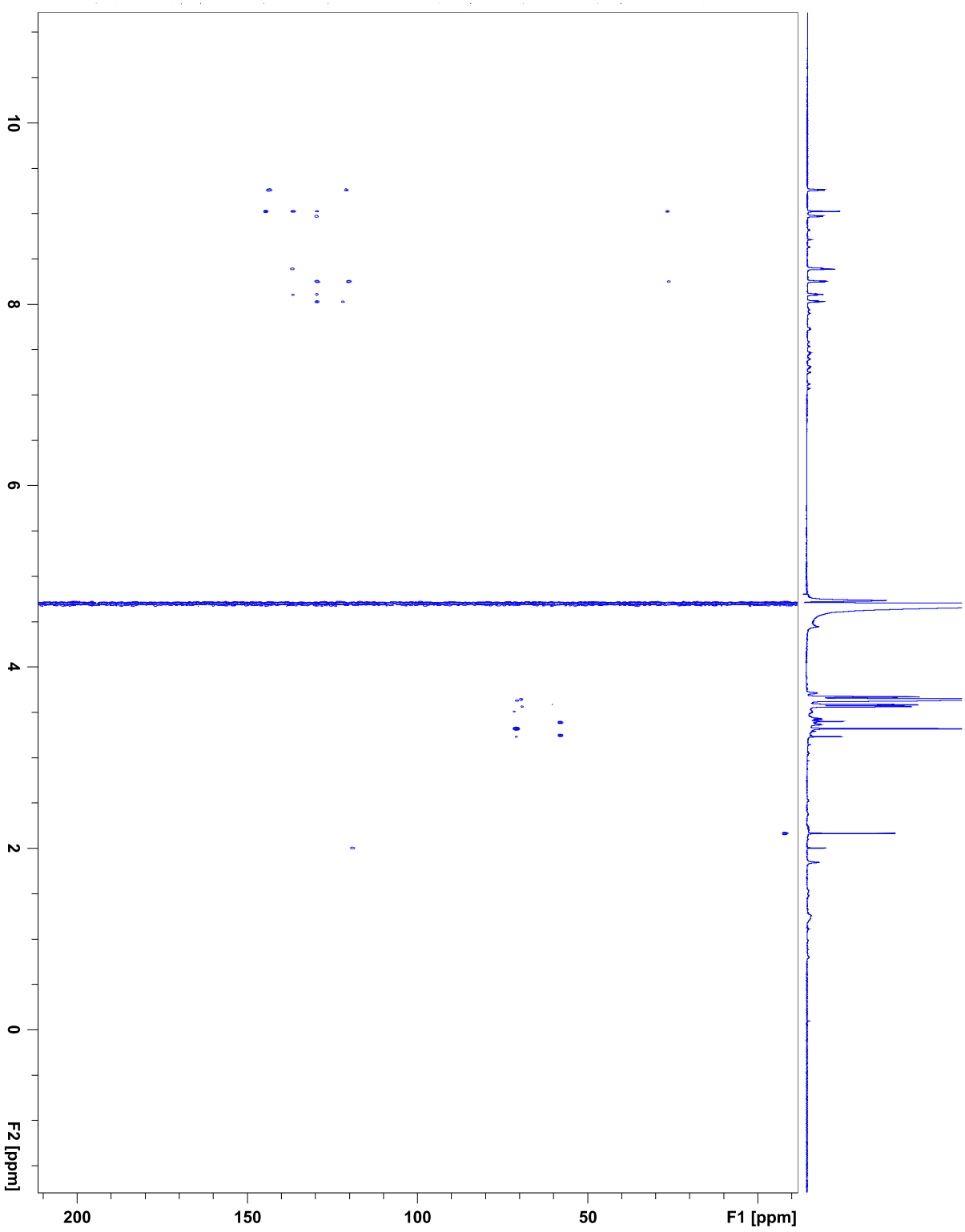

Figure S11 HMBC (H_2O + 10% D_2O, 1000.3 MHz) of **2**.

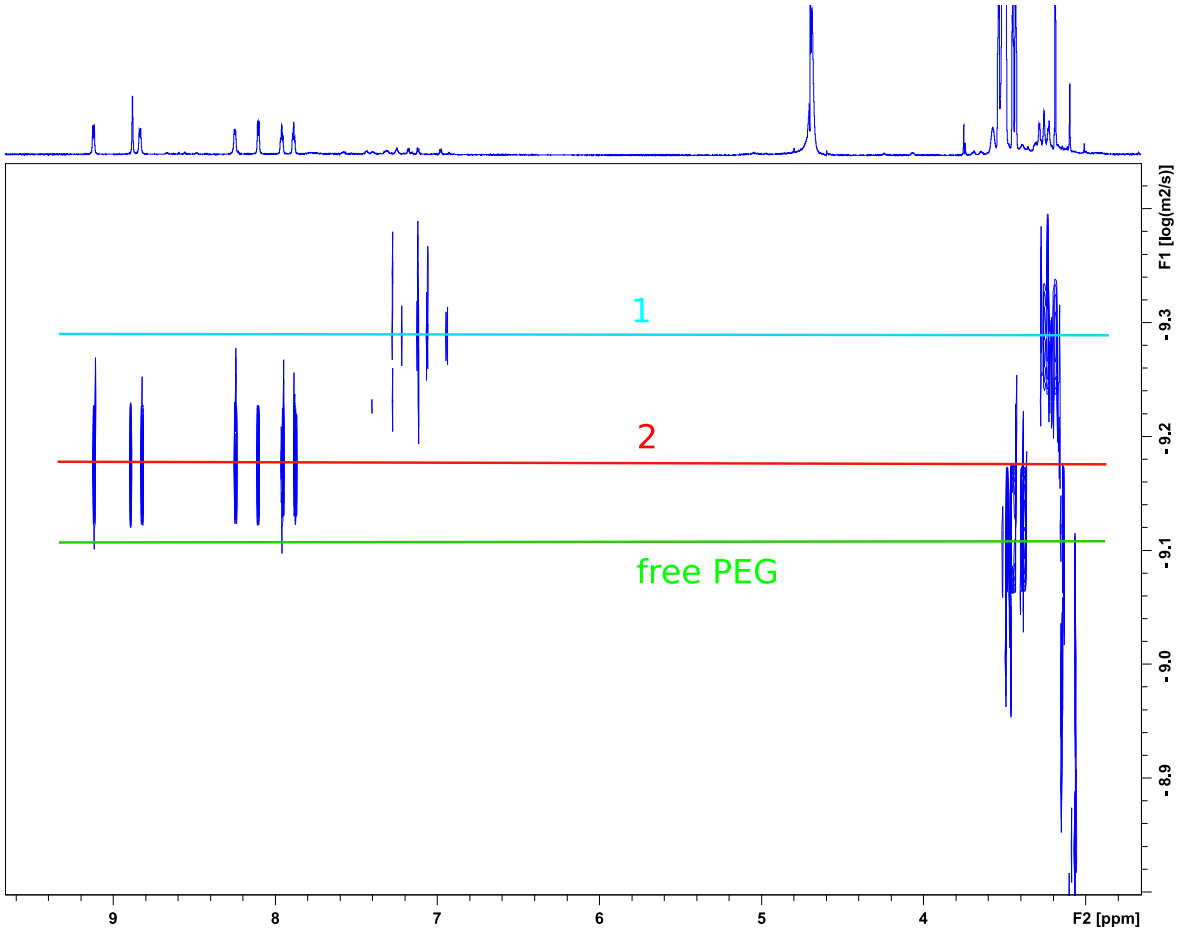

Figure S12 DOSY (H_2O + 10% D_2O, 1000.3 MHz) of **1**.

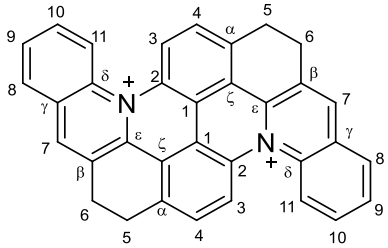

Table S1 Proton and carbon chemical shifts assignments of **2**. x : quaternary carbon, - : not assigned.

^{1}H or ^{13}C	Chemical shift (ppm)		Chemical shift (ppm)	
	^{1}H Exp.	^{1}H DFT	^{13}C Exp.	^{13}C DFT
3	9.27	9.61	129.91	131.84
4	8.26	8.89	130.06	131.69
5	3.67	4.10	26.09	21.21
6	3.72	4.10	26.57	21.55
7	9.03	9.67	142.71	145.55
8	8.40	9,17	129.61	132.34
9	8.03	8.89	130.29	131.50
10	8.11	8.95	133.15	135.54
11	8.98	9.61	121.93	122.23
1	x	x	121.10	123.17
2	x	x	129.60	130.36
α	x	x	143.73	147.79
β	x	x	-	-
γ	x	x	129.52	130.25
δ	x	x	136.70	137.65
ε	x	x	144.74	143.30
ζ	x	x	120.16	121.94

Spectra of **2 (procedure B)**

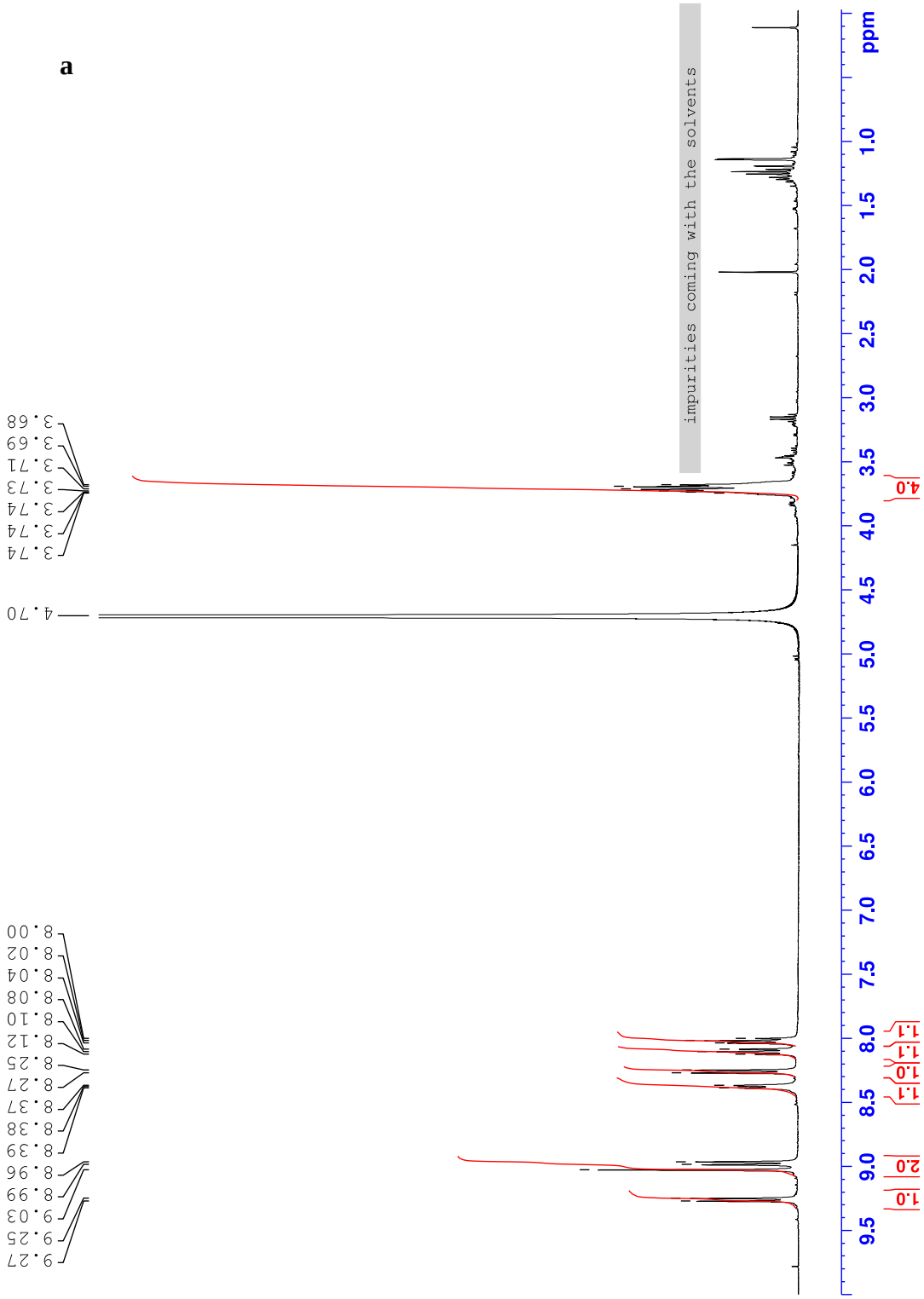

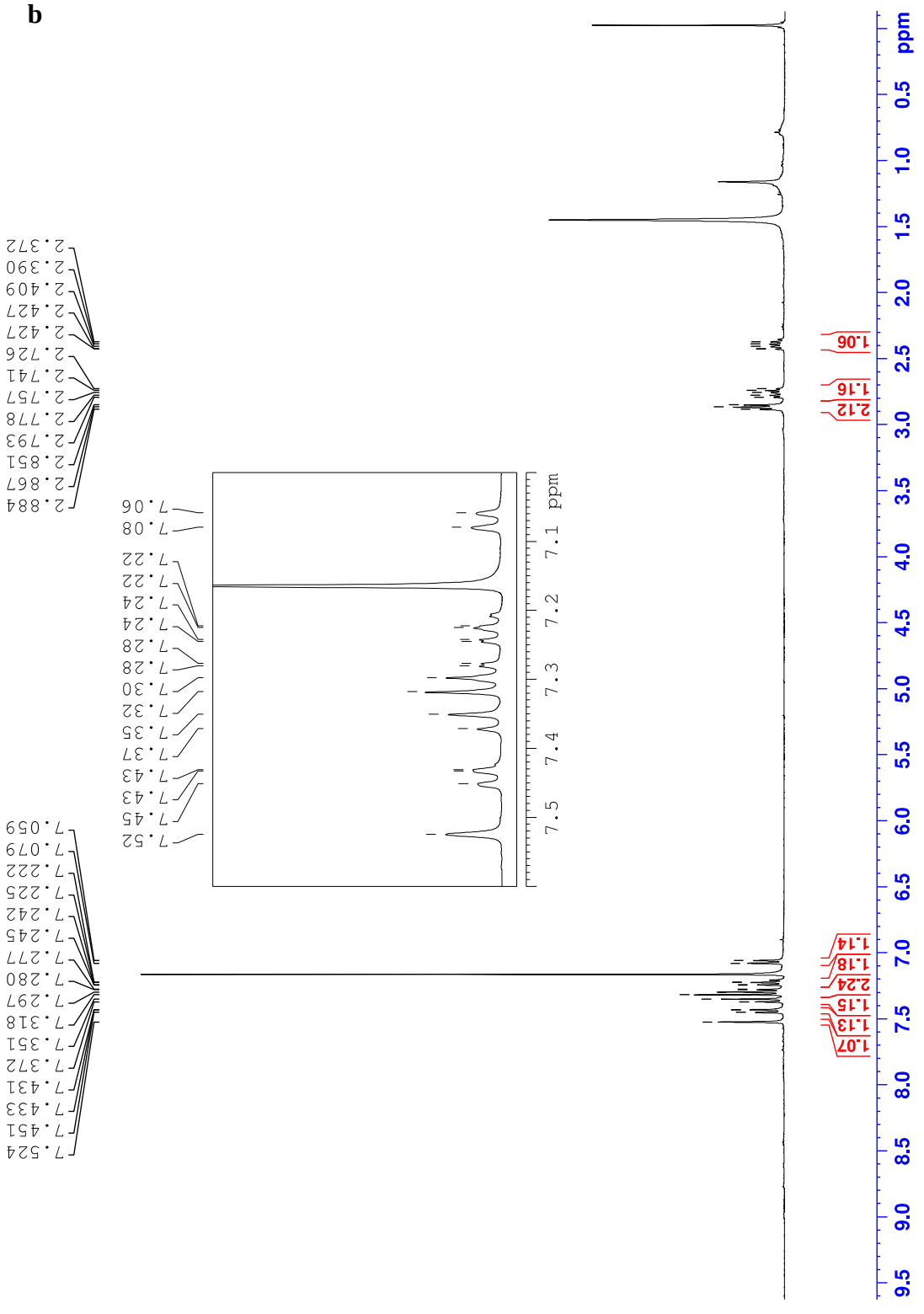

Figure S13 Spectrum **a**: ^{1}H NMR (D_2O, 400.140 MHz) spectrum of $\mathbf{2}^{2+}$, 2 Cl^- recovered from the aqueous phase and spectrum **b**: ^{1}H NMR ($CDCl_3$, 400.140 MHz) spectrum of **1'** extracted in the organic phase.

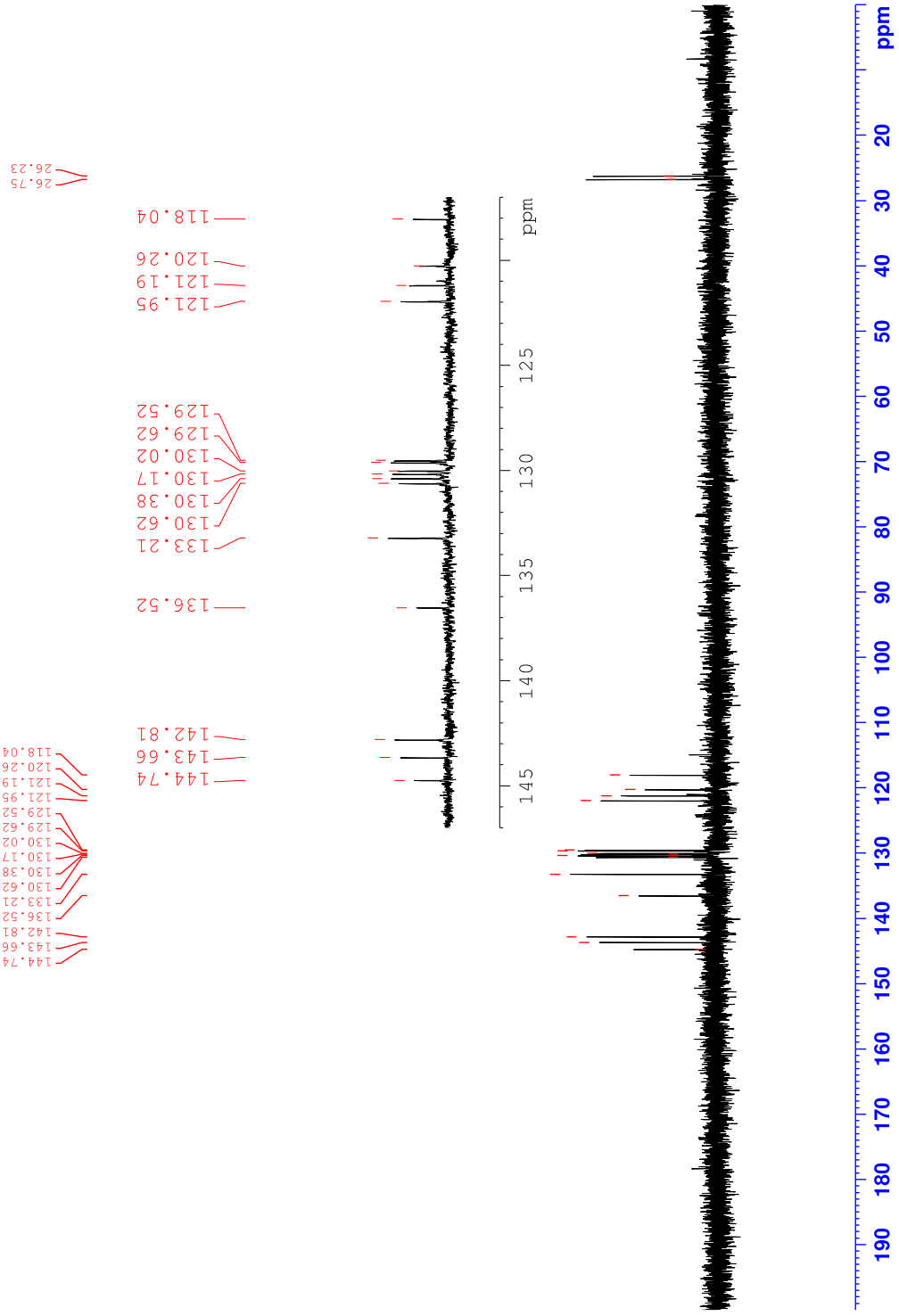

Figure S14 ^{13}C NMR (D_2O, 100.615 MHz) spectrum of $\mathbf{2}^{2+}$, 2 Cl^- recovered from the aqueous phase.

HPLC of 1’ to 2 conversion

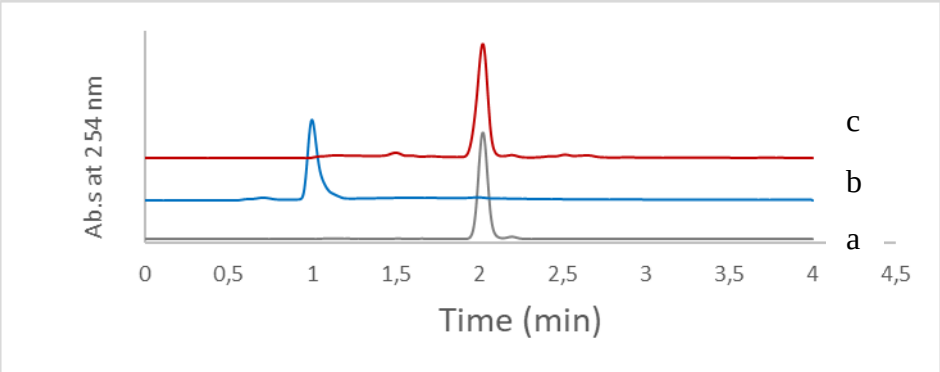

Figure S15 Chromatogram a: **1’** injected as the reference; Chromatogram b: aqueous phase (assigned to **2** regarding the corresponding m/z=229 peak); Chromatogram c: organic phase (assigned to **1’** in comparison to the reference chromatogram and regarding the corresponding m/z=757 peak).

Theoretical studies

NMR chemical shifts calculations

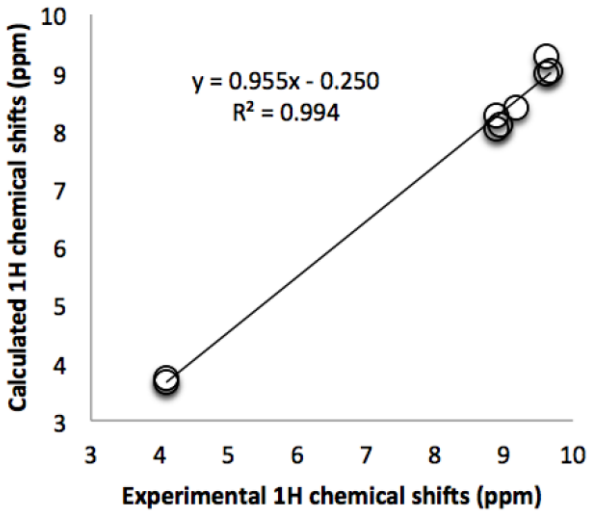

Figure S16 Exp. vs. computed ^{1}H NMR chemical shifts for **2**.

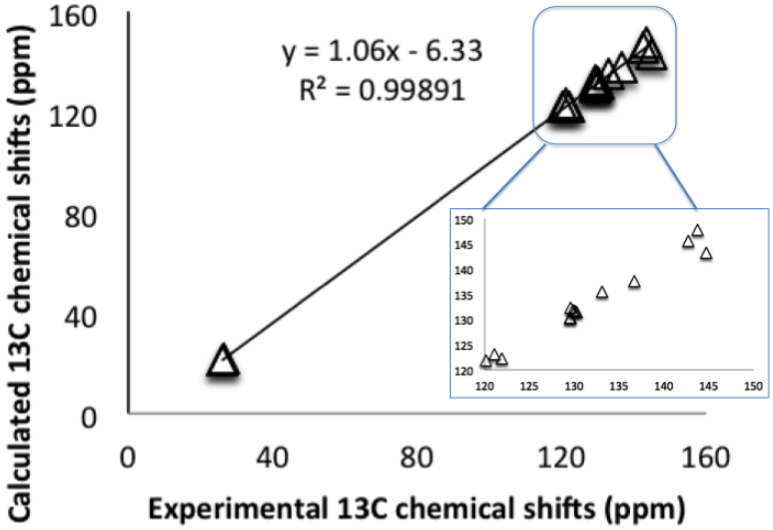

Figure S17 Exp. vs. computed ^{13}C NMR chemical shifts for **2** (with an inset for aromatic carbons).

TD-DFT simulated spectra

Molecular calculations were carried out with the Gaussian16 code.[1] The global hybrid functional PBE0 was used both for ground state and excited state geometry optimisations.[2] This functional was chosen because of its frequently reported accuracy for modelling the localized electronic transitions in organic molecules.[3] Structural optimizations and subsequent frequency calculations for both the ground and excited states were performed using an all electron Pople triple zeta basis set with one polarization function on all atoms and one diffuse function of heavier atoms, known as 6-31+G(d,p), for H, C, N and O atoms.[4,5] Bulk solvent effects were included using the Polarizable Continuum Model (PCM) of Tomasi and co-workers.[6] Default radii (from the UFF, scaled by 1.1) were used. Transitions in absorption were simulated by computing the first 10 transitions in TD-DFT at the same level of theory. The fluorescence energies were obtained by relaxing the first excited state geometry in TD-DFT at the same level of theory.

The Dalton[7] program was used to compute the SOC between the five first triplet states and the S1 state at the S1 optimized geometry using the quadric-response TD-DFT at the B3LYP/PCM level with the cc-pVDZ basis set adapted for the Douglas-Kroll calculations. The Spin-Orbit Coupling was computed using the Douglas-Kroll Hamiltonian along with the spin-orbit mean field approach, in an approach similar to our previously published works.[8] Vibrationally resolved spectra were obtained, after performing frequency calculations for the ground and excited states, using the FC classes program.[9] The reported spectra were simulated at 0K using convolution Gaussian function presenting a FWHM of 0.05 eV. 25 overtones for each mode and 20 combination bands were used as a maximum of 1010 integrals for each class.

From a TD-DFT point of view, the absorption spectrum of **1** is characterized by a series of weak transitions (oscillator strength < 0.04 a.u.) before reaching notably intense transitions (oscillator strength > 0.1 a.u.) around 330 nm thus corresponding to the main band observed experimentally (see Table S2). The weakly intense transitions are charge transfer transitions while the intense ones have a localized character (See Figure S18). This is quantified by the charge transfer index developed by Tozer, noted Λ, being around 0.5 for the first transitions while above 0.7 for the intense ones.[8] The simulated absorption spectra of **1** has a similar shape as the experimental one but blue-shifted with a deviation of 0.2 eV for the first intense transition, in the range of error expected for the PBE0 functional. The molecule **1** is probably not fluorescent because of the poorly emissive lowest singlet excited state having an oscillator strength below 0.01 a.u. On the contrary, the first singlet excited state of molecule **2** is

characterized by a strong oscillator strength (around 0.4 a.u.) explaining the strong fluorescent associated to this molecule. This transition in the visible part of the spectrum has a localized character, characterized by Λ index of 0.73. Simulated absorption spectra of the two compounds along with the electron density reorganization for some selected transitions are given below.

Table S2 Properties of the 10 first transitions computed by TD-DFT for molecule **1**.

Transition	λ (nm)	f (a.u.)	Orbital description
$S_0 \rightarrow S_1$	364	0.01	H → L: 86% H-2 → L: 14%
$S_0 \rightarrow S_2$	353	0.01	H → L+1: 65% H-1 → L: 24% H-2 → L+1: 12%
$S_0 \rightarrow S_3$	341	0.04	H-1 → L: 73% H → L+1: 27%
$S_0 \rightarrow S_4$	332	0.11	H-1 → L+1: 86% H → L: 14%
$S_0 \rightarrow S_5$	328	0.14	H-2 → L: 84% H → L: 16%
$S_0 \rightarrow S_6$	321	0.05	H-2 → L+1: 82% H → L+1: 17%
$S_0 \rightarrow S_7$	309	0.09	H-3 → L: 46% H-5 → L: 17%
$S_0 \rightarrow S_8$	308	0.11	H-3 → L+1: 47% H-4 → L: 18% H-5 → L+1: 14% H-7 → L: 13%
$S_0 \rightarrow S_9$	298	0.02	H-4 → L: 47% H-3→ L+1: 12% H-5 → L+1: 11% H-2 → L: 10%
$S_0 \rightarrow S_{10}$	294	0.00	H-4 → L+1: 34% H-5→ L: 25% H-2 → L+3: 10% H-6 → L: 10% H-2 → L+1: 10%

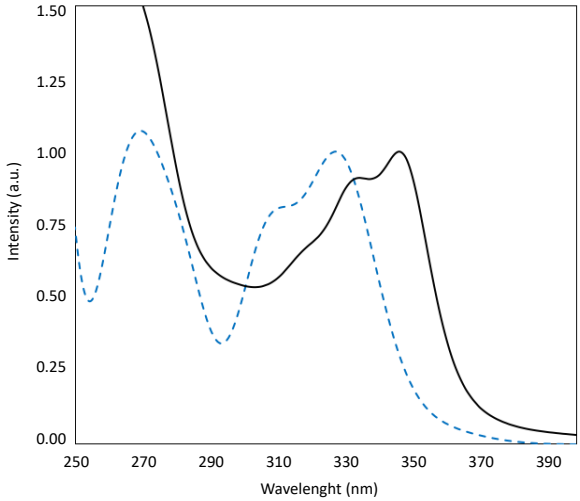

Figure S18 Experimental (black full line) and simulated (blue dotted line) absorption spectra of **1**. The simulation is done by convoluting TD-DFT stick spectrum with gaussian functions (FWHM=0.25 eV).

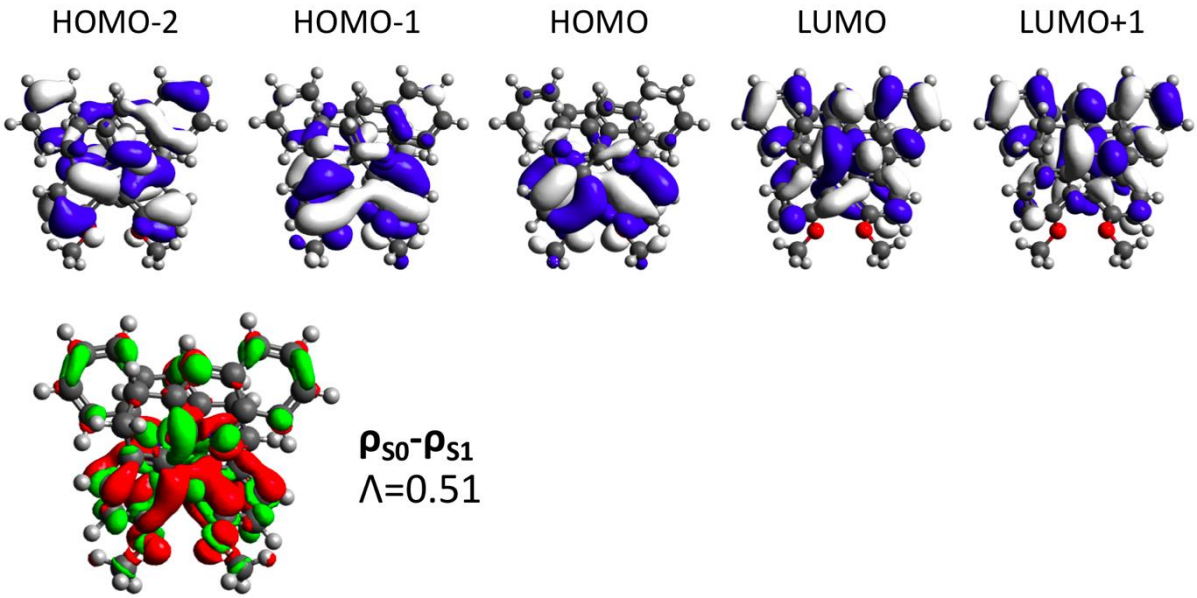

Figure S19 Selected orbitals involved in the electronic transitions (isocontour 0.03 a.u.) and variation of the electron density for the first transition (green and red areas corresponding to electron density increase and decrease respectively, isocontour 0.001 a.u.) of molecule **1**. The Tozer index, Λ, is also given for this transition.

Table S3 Properties of the 10 first transitions computed by TD-DFT for molecule **2**.

Transition	λ (nm)	f (a.u.)	Orbital description
$S_0 \rightarrow S_1$	409	0.37	H → L : 55% H-2 → L : 35%
$S_0 \rightarrow S_2$	390	0.02	H-1 → L : 100%
$S_0 \rightarrow S_3$	387	0.28	H-2 → L : 56% H → L : 34% H → L+2 : 10%
$S_0 \rightarrow S_4$	376	0.00	H → L+1 : 65% H-1 → L+1 : 35%
$S_0 \rightarrow S_5$	356	0.28	H-1 → L+1 : 70% H-3 → L : 30%
$S_0 \rightarrow S_6$	354	0.01	H-2 → L+1 : 66% H → L+1 : 34%
$S_0 \rightarrow S_7$	332	9.04	H-3 → L : 48% H-1 → L+1 : 20% H-2 → L+2 : 11% H-4 → L+1 : 11% H → L+2 : 10%
$S_0 \rightarrow S_8$	326	0.01	H-4 → L : 63% H-3 → L+1 : 17% H → L+2 : 10%
$S_0 \rightarrow S_9$	303	0.05	H-4 → L+1 : 43% H→ L+2 : 26% H-3 → L: 13% H-1 → L+2: 12%
$S_0 \rightarrow S_{10}$	303	0.00	H-3 → L+1 : 80% H-4→ L : 20%

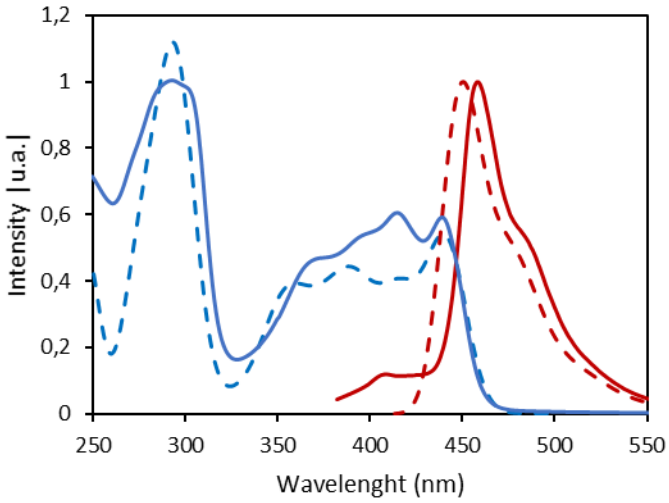

Figure S20 Experimental (full lines) and simulated (dotted lines) absorption (blue) and fluorescence (red) spectra of **2**. For the absorption spectrum, the simulation is done by convoluting TD-DFT stick spectrum with gaussian function (FWHM=0.25 eV) but for the first transition, the convoluted vibronic transitions were used (FWHM=0.05 eV). For the fluorescence spectrum, the convoluted vibronic transitions were used (FWHM=0.05 eV).

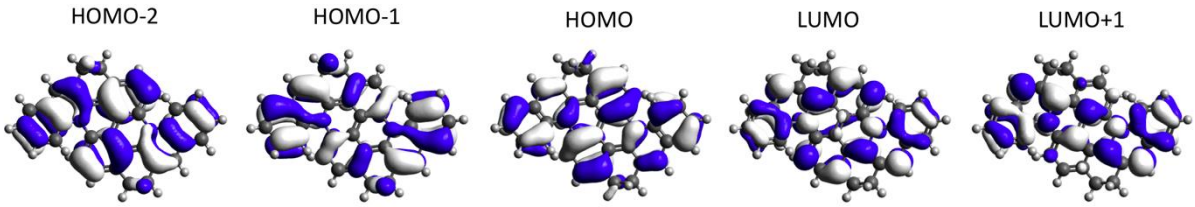

Figure S21 Selected orbitals involved in the electronic transitions (isocontour 0.03 a.u.) of molecule **2**.

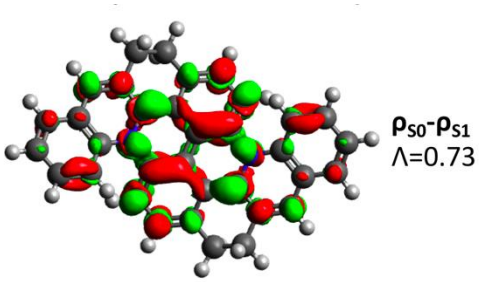

Figure S22 Variation of the electron density for the first transition (green and red areas corresponding to electron density increase and decrease respectively, isocontour 0.001 a.u.) of molecule **2**. The Tozer index, Λ, is also given for this transition.

Spectra associated to the study of the photochemical reaction

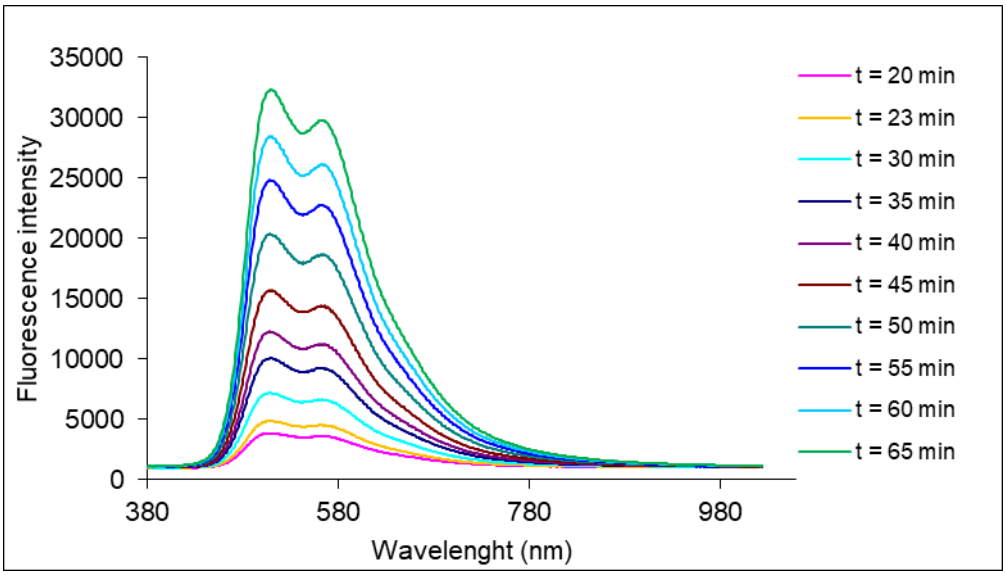

Figure S23 Evolution of the emission during irradiation at 350 nm of a solution of **1** in water.

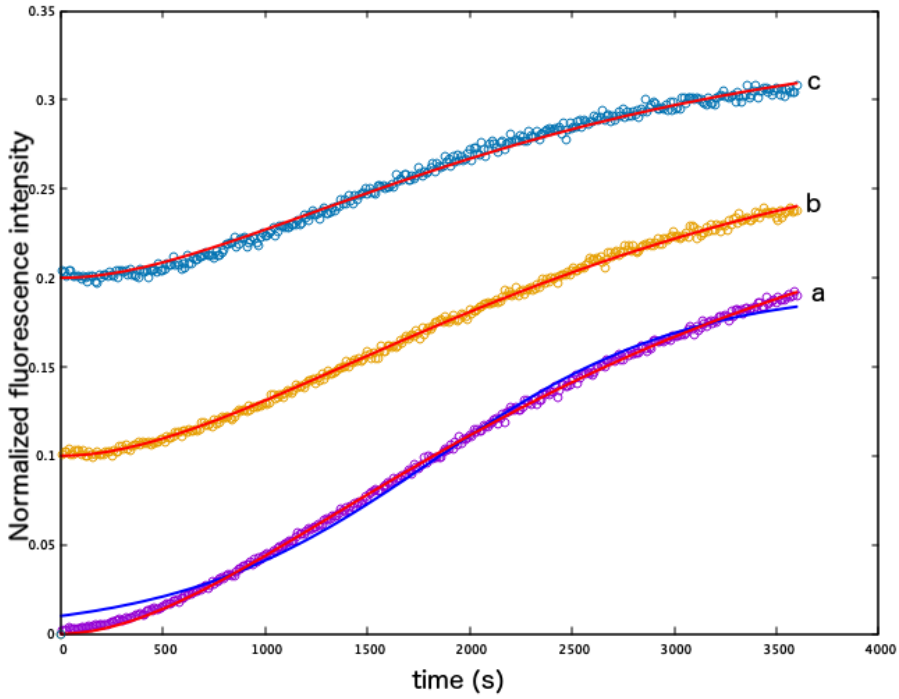

Figure S24 Kinetic of the reaction upon irradiation at 350 nm in a water solution of **1** (a), in **1**+**2** (b) and in **1**+**2** (c) increasing the amount of **2**. Kinetic (a) is moderately well fitted by the autocatalytic model (blue curve): $[2] = ([2]_{0+}\,[1]_{0)} / [([1]_0/[2]_0)\, e^{\,-([1]_0+\,[2]_0)\,kt} + 1]$. Kinetics (a), (b), (c) are well fitted by the kinetic model for two successive reactions (red curves): $[2] = [1]_0\,[1 - (k_2\, e^{-k_1 t} - k_1\, e^{-k_2 t}) / (k_2 - k_1)]$.

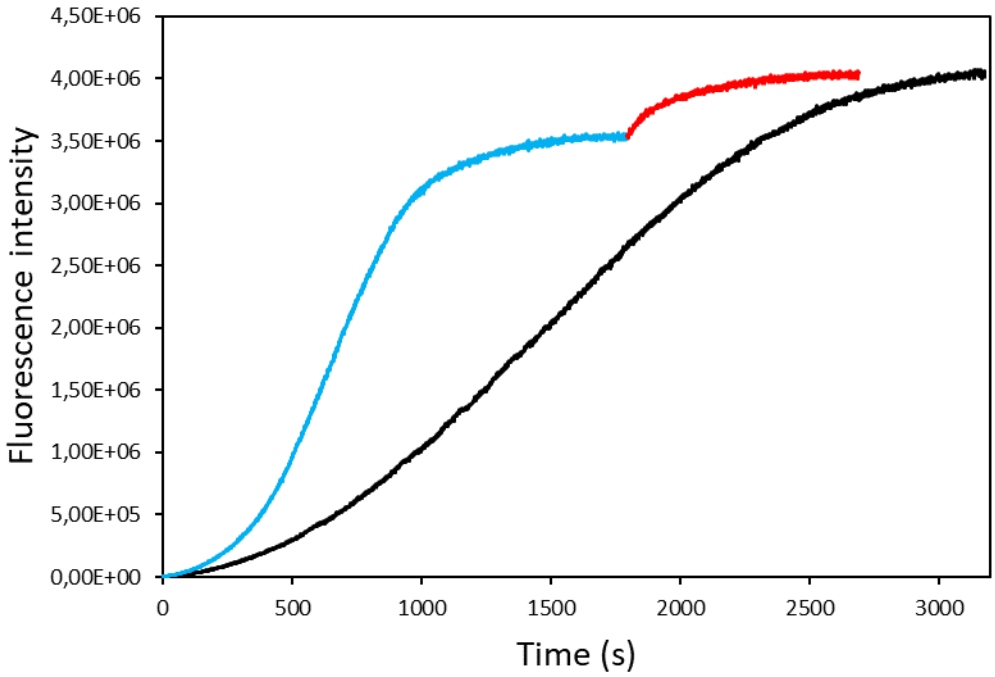

Figure S25 Kinetic of the reaction upon irradiation at 350 nm in a water solution of **1** (black), in a partially degassed water solution of **1** (blue) and after reoxygenation (red).

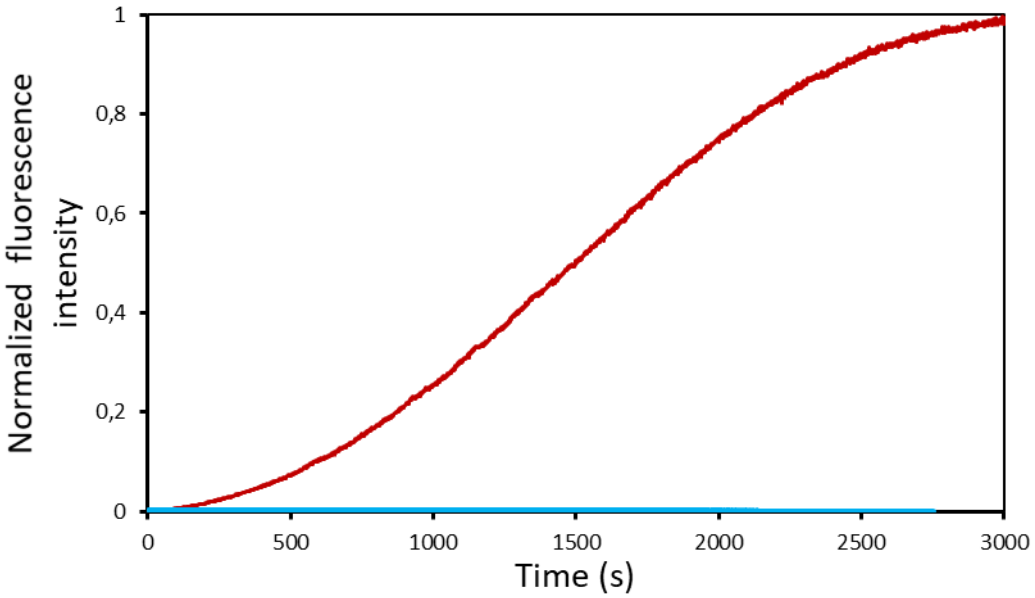

Figure S26 Kinetic of the reaction in a water solution of **1** upon irradiation at 350 nm (red), upon irradiation at 414 nm (blue).

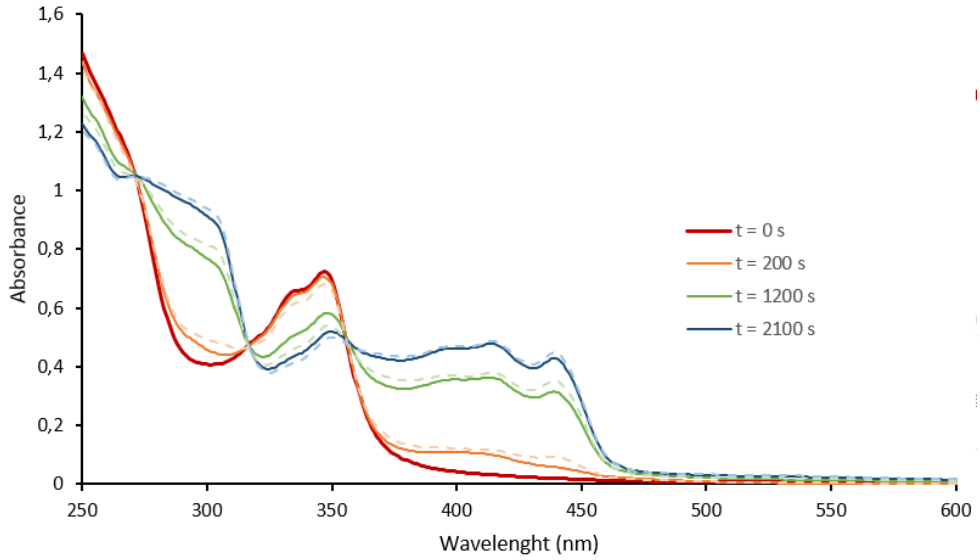

Figure S27 Series of irradiations of a solution of **1** in deionized water at 350 nm and 414 nm. Red line: initial absorption spectrum. Orange plain line represents the absorption spectrum after 200 s of irradiation at 350 nm; orange dashed line represents the spectrum of the solution irradiated 200s at 350 nm + 200 s at 414 nm. Green plain line irradiated 200 s at 350 nm + 200 s at 414 nm + 1000 s at 350 nm, green dashed line represents 200 s at 350 nm + 200 s at 414 nm + 1000 s at 350 nm + 1000 s at 414 nm. Blue plain line represents the spectrum of the solution irradiated 200 s at 350 nm + 200 s at 414 nm + 1000 s at 350 nm + 1000 s at 414 nm + 900 s at 350 nm, blue dashed line represents 200 s at 350 nm + 200s at 414 nm + 1000 s at 350 nm + 200 s at 414 nm + 900 s at 350 nm+ 900 s at 414 nm.

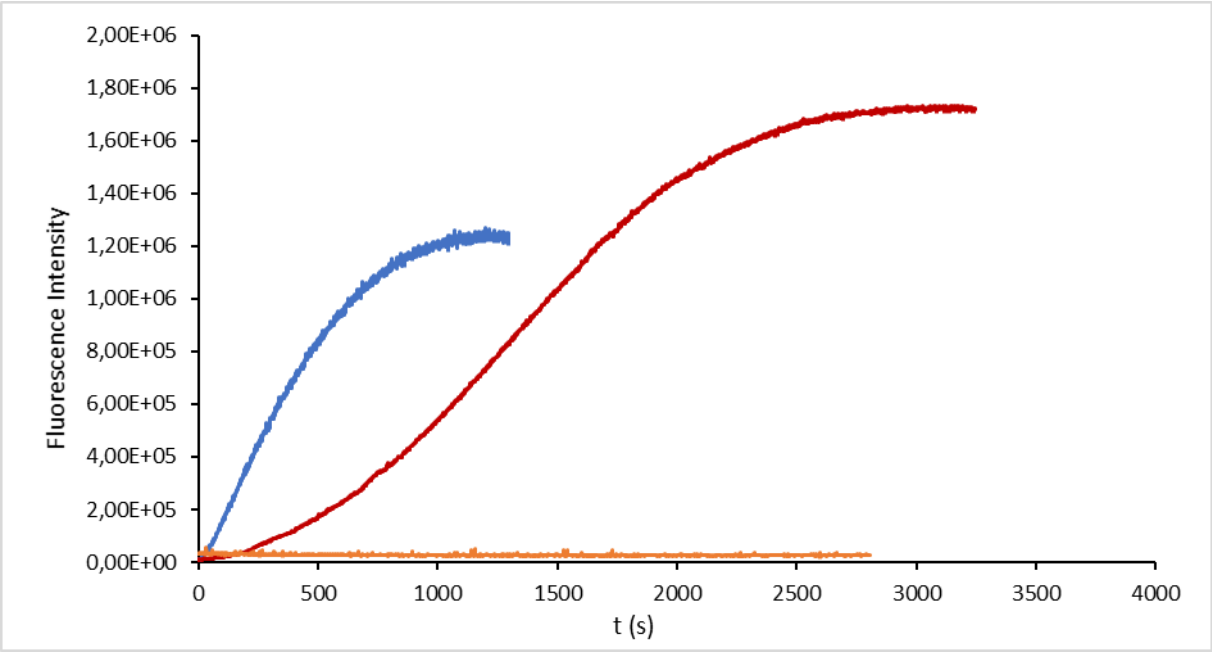

Figure S28 Compared kinetics of **1** and **1'**. Blue: reaction of **1'** (c = 45 μM) in CH_2Cl_2 , red: reaction of **1** (c = 45 μM) in water, orange: reaction of **1** (c = 45 μM) in CH_2Cl_2 upon irradiation at 350 nm.

G4-binding studies

Oligonucleotide annealing and morphological characterization

Table S4 List of the G4 and non-G4 oligonucleotides used in this study.

Name	Sequence 5'-3'	Length (bp)	Molar extinction coefficient ($M^{-1}cm^{-1}$)[a]	GC %	Topology and description
c-MYC Pu22	TGAGGGTGGGTAGGGTGGGTAA	22	228700	59.1	parallel
Tel-22	AGGGTTAGGGTTAGGGTTAGGG	22	228500	54.5	hybrid/anti-parallel
Bom17	GGTTAGGTTAGGTTAGG	17	174600	47.1	anti-parallel
$4G_3U_3$	GGGUUUGGGUUUGGGUUUGGG	21	185600	57.1	parallel
ds-DNA	CAATCGGATCGAATTCGATCCGATTG	26	253200	46.2	double stranded
scr-ds-DNA[b]	ATGACTGAGACTGAGGCTACAT ATGTAGCCTCAGTCTCAGTCAT	22	/	45.5	double stranded
GC-rich ds-DNA[b]	GGGTGGGTAGGGTGGG CCCACCCTACCCACCC	16	/	75.0	double stranded
ds-RNA	CAGUACAGAUCUGUACUG	18	170500	44.4	double stranded
ss-DNA	TTACCCACCCTACCCACCCTCA	22	191500	59.1	single stranded
i-motif[c]	TTACCCACCCTACCCACCCTCA	22	191500	59.1	/

[a]Molar extinction coefficient calculated by using oligo analyzer on the IDT web site. [b]scr-ds-DNA and GC-rich ds-DNA were annealed by mixing an equimolar concentration of each strand. [c]i-motif formation was induced in cacodylate buffer (pH 5.0).

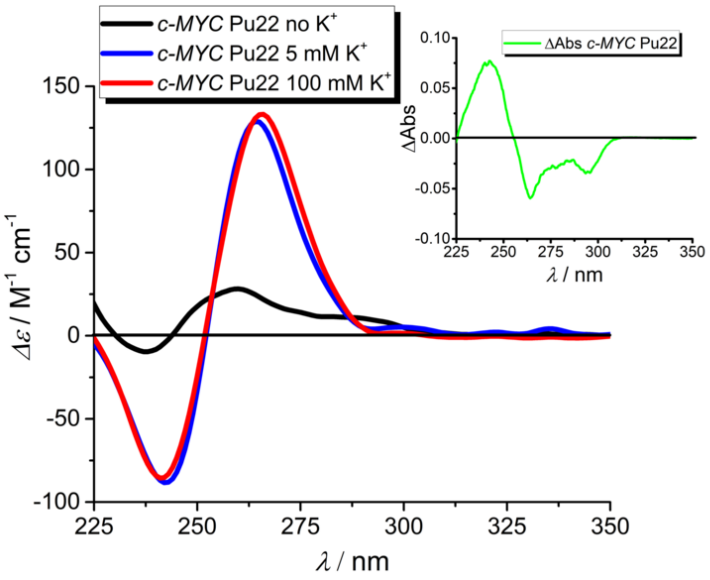

Figure S29 ECD spectra of *c-MYC* Pu22 ($C_{c\text{-}MYC\ PU22}$ = 2 μM) in the absence (black line) and presence of K^+ (blue and red lines). Inset: IDS of *c-MYC* Pu22 (green line). All the measurements were performed in C_{Tris} = 10 mM pH 7.4, C_{KCl} = 0, 5 or 100 mM.

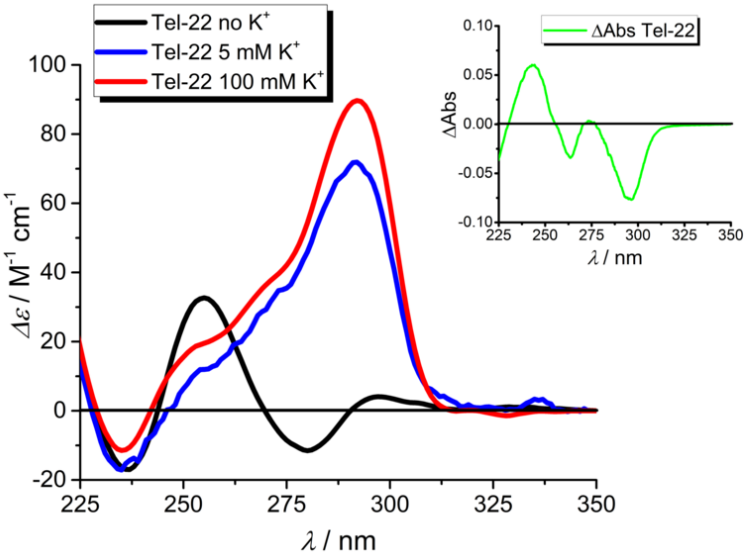

Figure S30 ECD spectra of Tel-22 ($C_{Tel\text{-}22}$ = 2 μM) in the absence (black line) and presence of K^+ (blue and red lines). Inset: IDS of Tel-22 (green line). All the measurements were performed in C_{Tris} = 10 mM pH 7.4, C_{KCl} = 0, 5 or 100 mM.

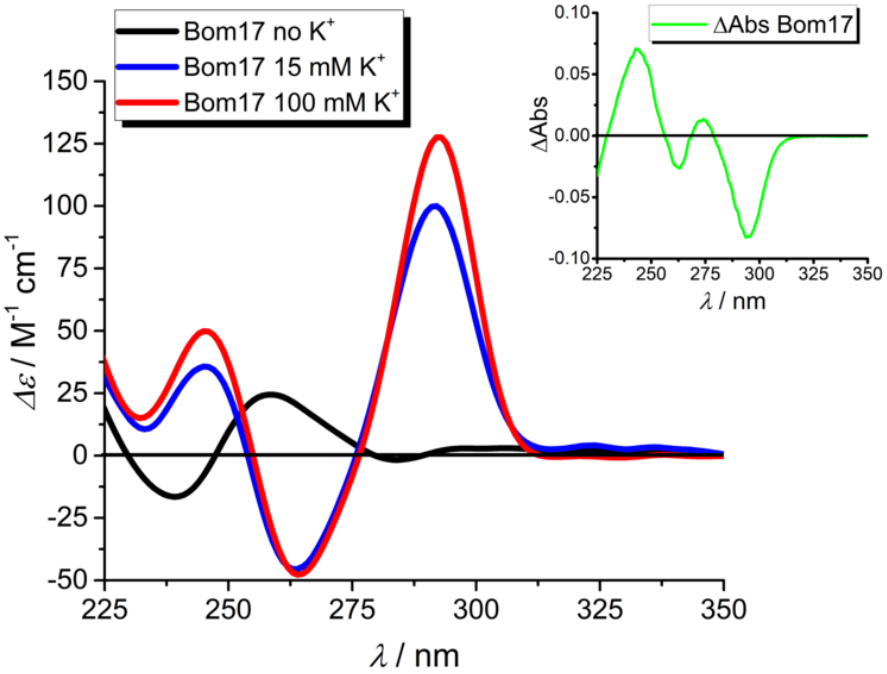

Figure S31 ECD spectra of Bom17 (C_{Bom17} = 2 μM) in the absence (black line) and presence of K^+ (blue and red lines). Inset: IDS of Bom17 (green line). All the measurements were performed in C_{Tris} = 10 mM pH 7.4, C_{KCl} = 0, 15 or 100 mM.

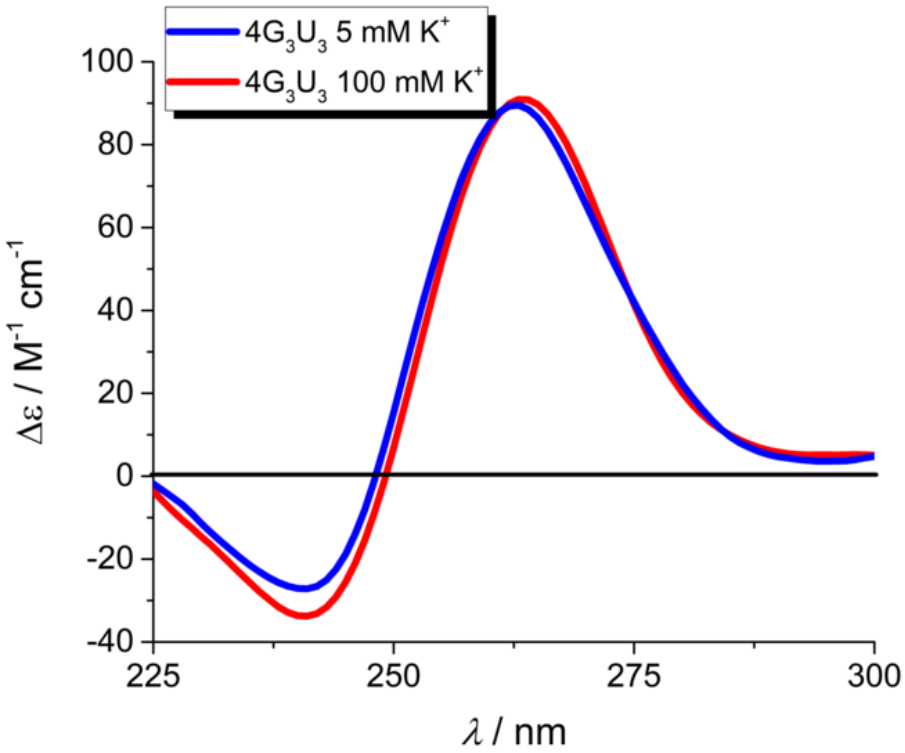

Figure S32 ECD spectra of $4G_3U_3$ (C_{4G3U3} = 2 μM) in the presence of 5 mM K^+ (blue line) or 100 mM K^+ (red line). All the measurements were performed in C_{Tris} = 10 mM pH 7.4, C_{KCl} = 5 or 100 mM.

Photoconversion in buffered solution

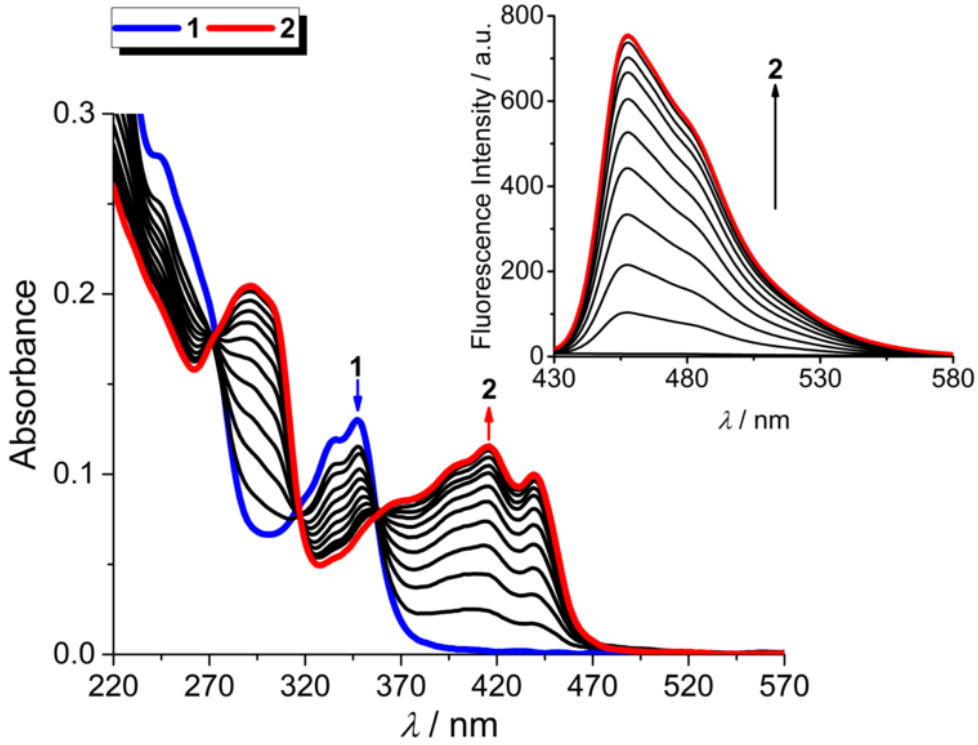

Figure S33 Photoconversion of **1** into **2** upon excitation at 350 nm. (C_1 = 3.8 µM, C_{KCl} = 100 mM, C_{Tris} = 50 mM pH7.4).

Titration experiments

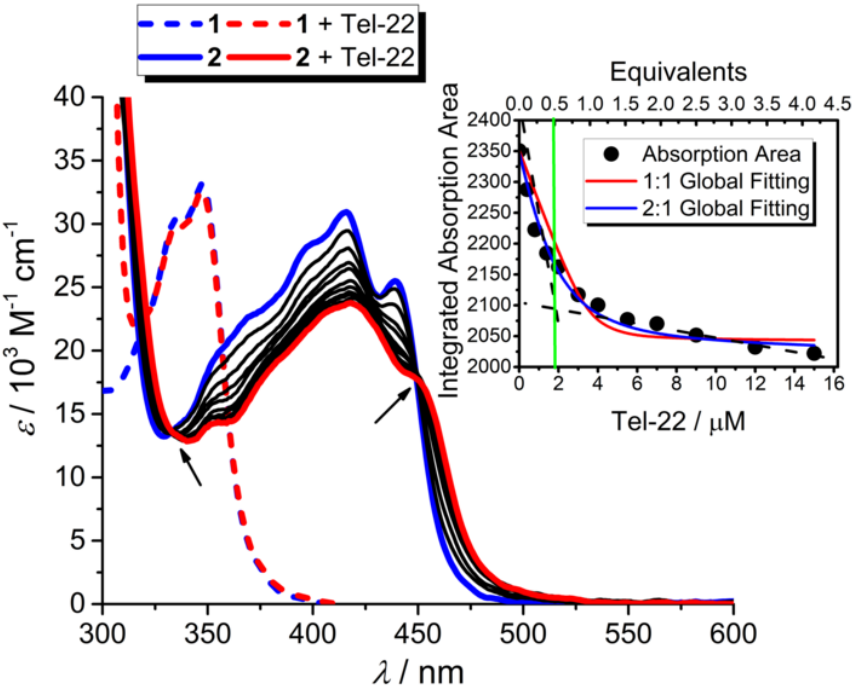

Figure S34 UV/Vis absorption spectra of **1** (dashed lines) and **2** (solid lines) in the presence of Tel-22 (C_1 = 3.8 µM, C_2 = 3.6 µM, C_{Tel-22} = 0 to 15 µM, C_{KCl} = 100 mM, C_{Tris} = 50 mM pH 7.4). The arrows indicate the isosbestic points. Inset: nonlinear fitting procedure obtained by using a global 1:1 and noncooperative 2:1 binding model. The dashed black and the vertical green lines aim to show the inflection point supporting a 2:1 binding stoichiometry.

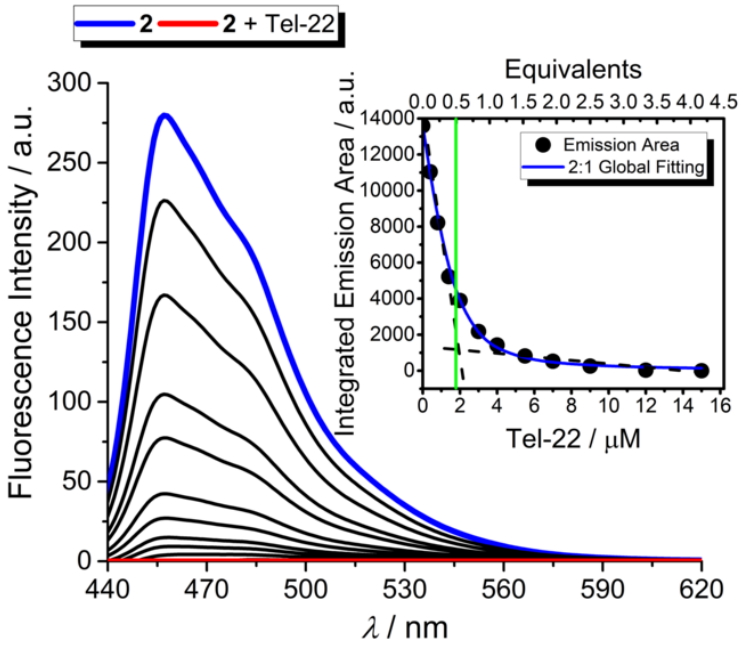

Figure S35 Emission spectra of **2** in the presence of Tel-22 (C_2 = 3.6 μM, $C_{Tel\text{-}22}$ = 0 to 15 μM, C_{KCl} = 100 mM, C_{Tris} = 50 mM pH 7.4, λ_{exc} = 328 nm). Inset: nonlinear fitting procedure obtained by using a global noncooperative 2:1 binding model. The dashed black and the vertical green lines indicate the inflection point supporting a 2:1 binding stoichiometry.

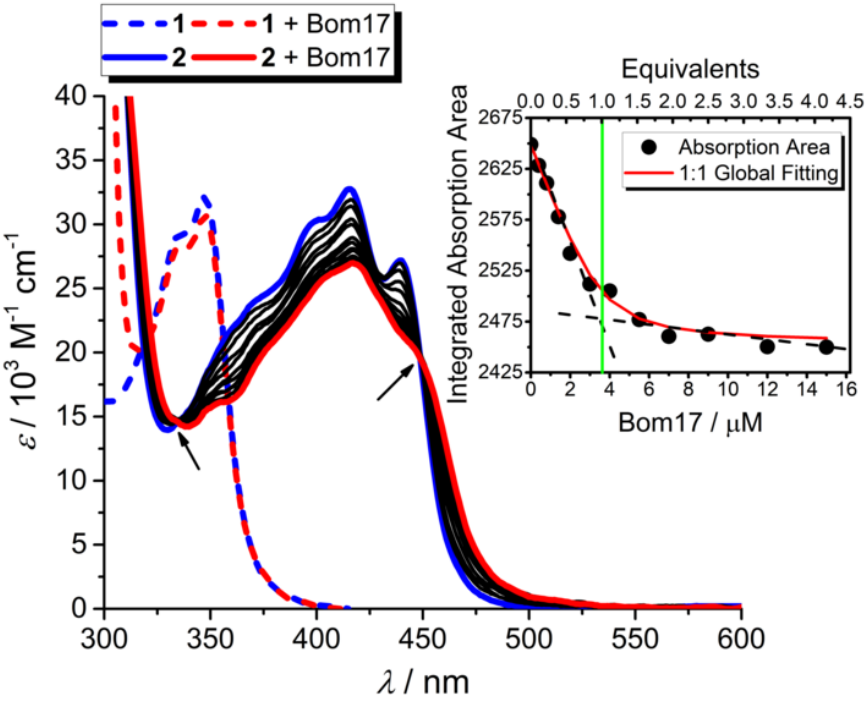

Figure S36 UV/Vis absorption spectra of **1** (dashed lines) and **2** (solid lines) in the presence of Bom17 (C_1 = 3.8 μM, C_2 = 3.6 μM, C_{Bom17} = 0 to 15 μM, C_{KCl} = 100 mM, C_{Tris} = 50 mM pH 7.4). The arrows indicate the isosbestic points. Inset: nonlinear fitting procedure obtained by using a global 1:1 binding model. The dashed black and the vertical green lines aim to show the inflection point supporting a 1:1 binding stoichiometry.

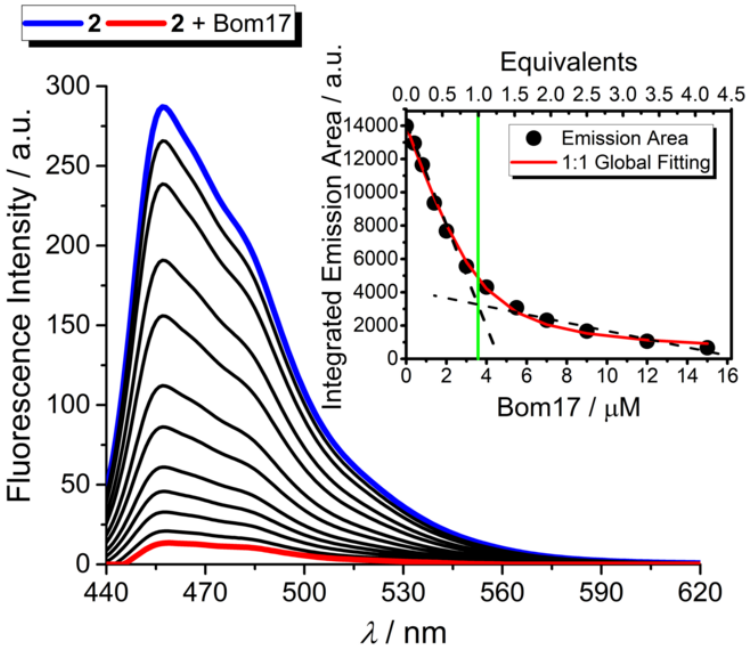

Figure S37 Emission spectra of **2** in the presence of Bom17 (C_2 = 3.6 μM, C_{Bom17} = 0 to 15 μM, C_{KCl} = 100 mM, C_{Tris} = 50 mM pH 7.4, λ_{exc} = 328 nm). Inset: nonlinear fitting procedure obtained by using a global 1:1 binding model. The dashed black and the vertical green lines indicate the inflection point supporting a 1:1 binding stoichiometry.

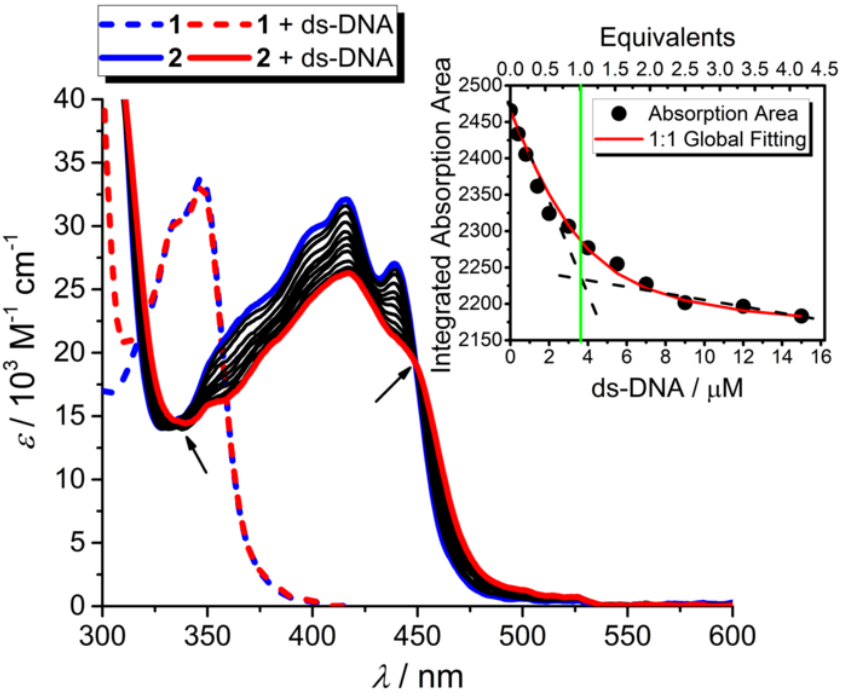

Figure S38 UV/Vis absorption spectra of **1** (dotted lines) and **2** (solid lines) in the presence of ds-DNA (C_1 = 3.8 μM, C_2 = 3.6 μM, $C_{ds\text{-}DNA}$ = 0 to 15 μM, C_{KCl} = 100 mM, C_{Tris} = 50 mM pH 7.4). The arrows indicate the isosbestic points. Inset: nonlinear fitting procedure obtained by using a global 1:1 binding model. The dashed black and the vertical green lines aim to show the inflection point supporting a 1:1 binding stoichiometry.

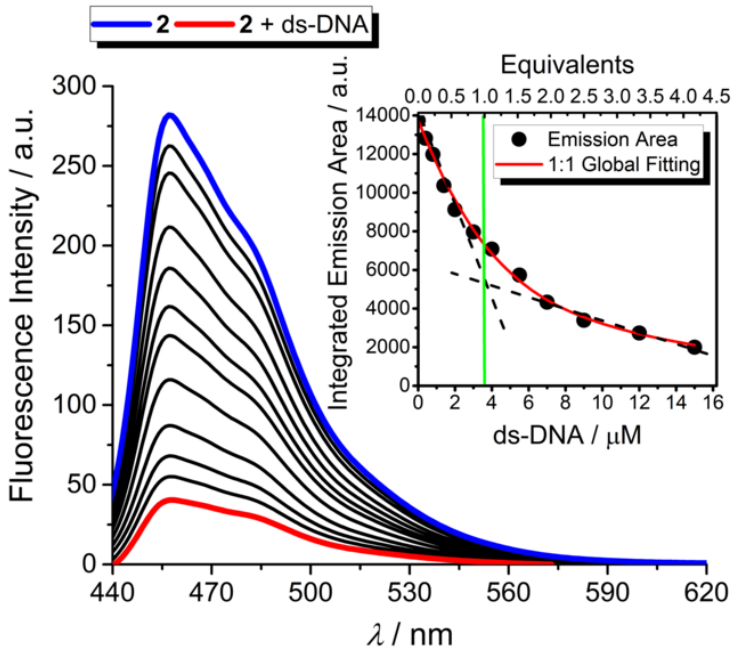

Figure S39 Emission spectra of **2** in the presence of ds-DNA (C_2 = 3.6 μM, $C_{ds\text{-}DNA}$ = 0 to 15 μM, C_{KCl} = 100 mM, C_{Tris} = 50 mM pH 7.4, λ_{exc} = 328 nm). Inset: nonlinear fitting procedure obtained by using a global 1:1 binding model. The dashed black and the vertical green lines indicate the inflection point supporting a 1:1 binding stoichiometry.

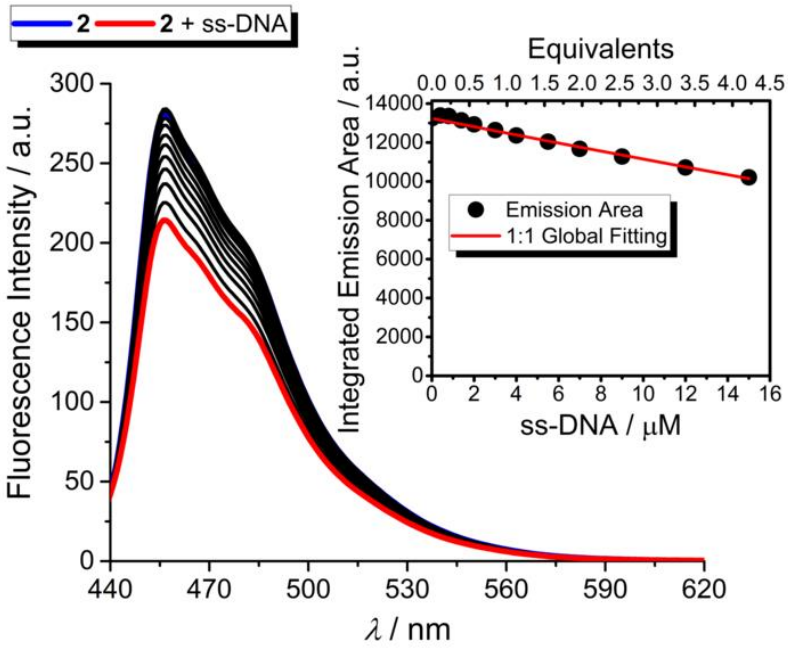

Figure S40 Emission spectra of **2** in the presence of ss-DNA (C_2 = 3.6 μM, $C_{ss\text{-}DNA}$ = 0 to 15 μM, C_{KCl} = 100 mM, C_{Tris} = 50 mM pH 7.4, λ_{exc} = 328 nm). Inset: nonlinear fitting procedure obtained by using a global 1:1 binding model. No quantitative data analysis is performed due to the weak optical changes and the lack of a fully saturated system.

i-motif formation

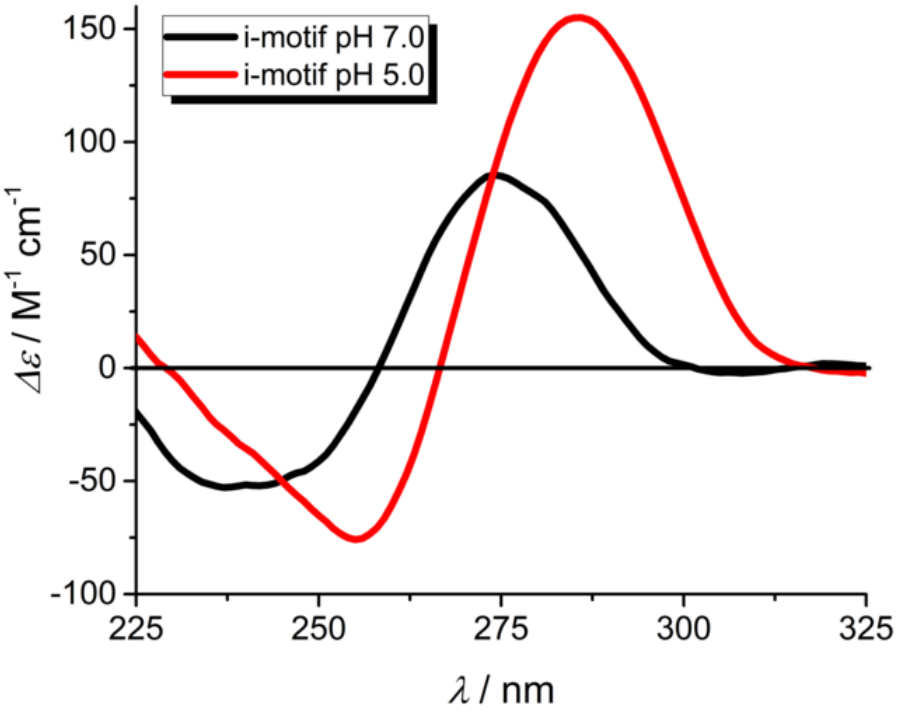

Figure S41 ECD spectra showing the formation of the i-motif structure ($C_{i\text{-motif}}$) = 2 μM obtained at pH 5.0. All the measurements were performed in $C_{cacodylate\ buffer}$ = 50 mM (pH 7.0 or pH 5.0) and C_{KCl} = 100 mM.

^{1}H NMR Titration studies

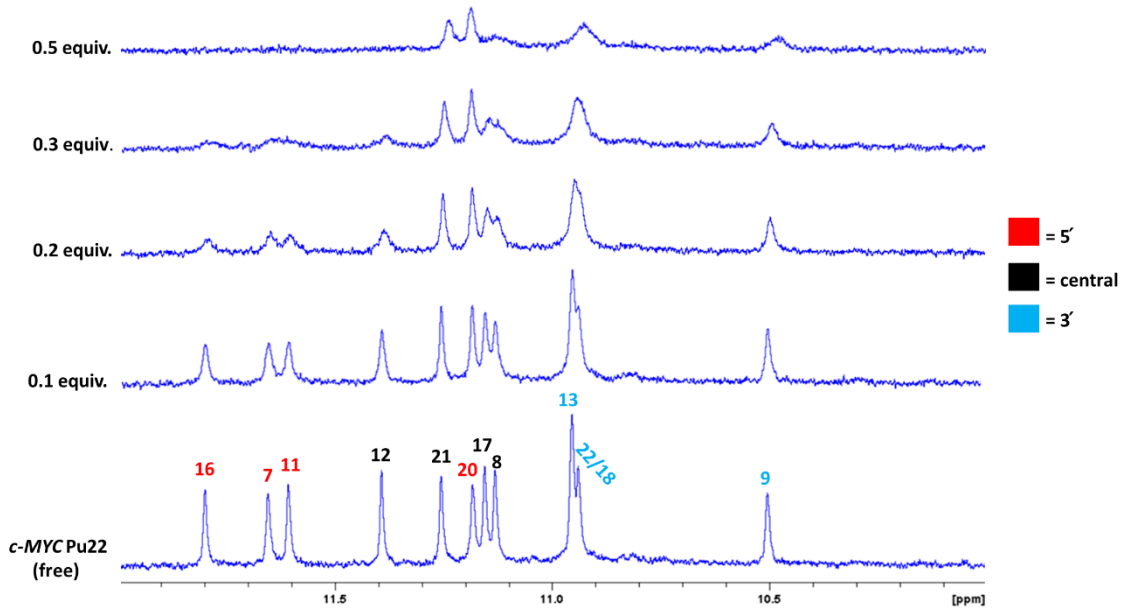

Figure S42 1D ^{1}H NMR titrations for *c-MYC* Pu22 with **2** at different **2**/*c-MYC* Pu22 ratios. The guanines involved into the formation of the G4 structure are color coded. ($C_{c\text{-}MYC\ Pu22}$ = 90 μM, C_2 = 0 to 45 μM, C_{KCl} = 35 mM, C_{buffer} = 10 mM pH 7.4).

ECD spectra of **2** with G4 templates

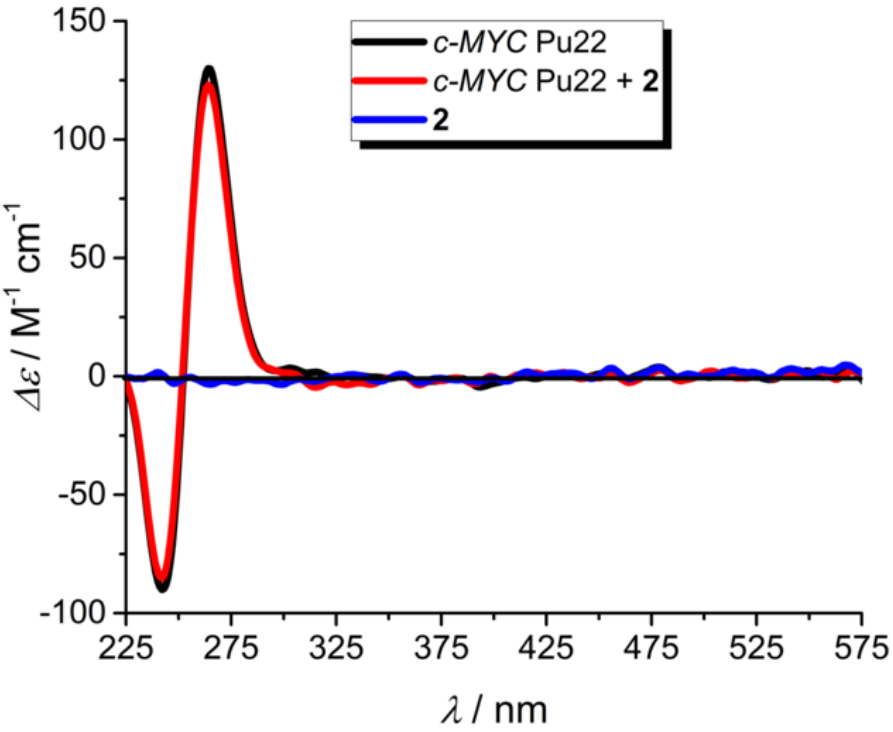

Figure S43 ECD spectra of *c-MYC* Pu22 upon addition of **2** (black and red lines correspond to the spectra at 0.0 eq. and 1.0 eq., respectively). **2** is CD silent as shown by the blue line (C_2 = 2.0 µM, $C_{c\text{-}MYC\ Pu22}$ = 2.0 µM, C_{KCl} = 100 mM, C_{Tris} = 50 mM pH 7.4).

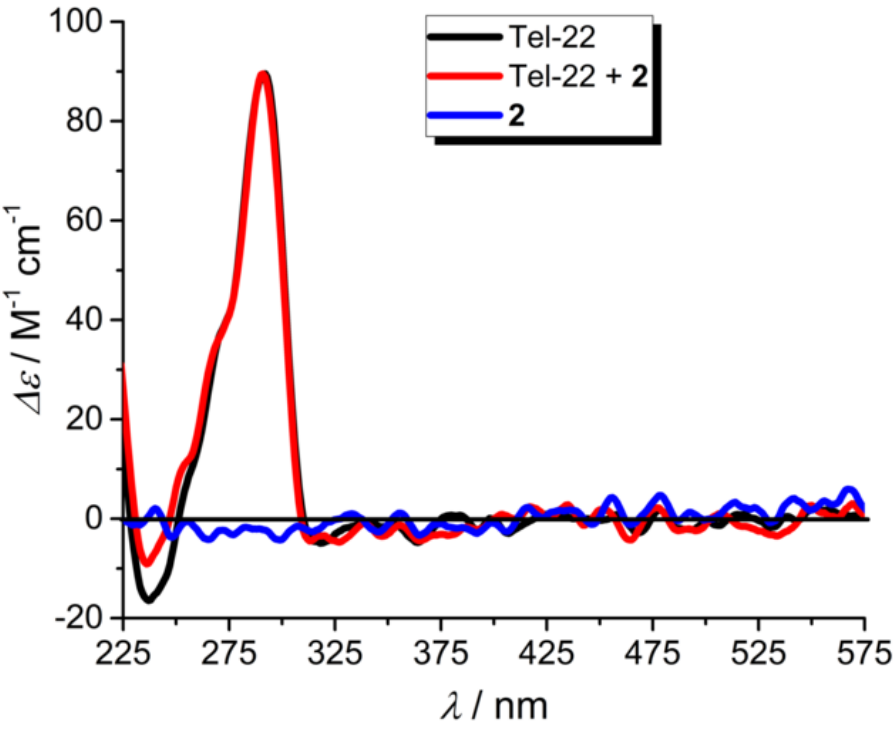

Figure S44 ECD spectra of Tel-22 upon addition of **2** (black and red lines correspond to the spectra at 0.0 eq. and 1.0 eq., respectively). **2** is CD silent as shown by the blue line (C_2 = 2.0 µM, $C_{c\text{-}MYC\ Pu22}$ = 2.0 µM, C_{KCl} = 100 mM, C_{Tris} = 50 mM pH 7.4).

Phen-DC_3 competition assay

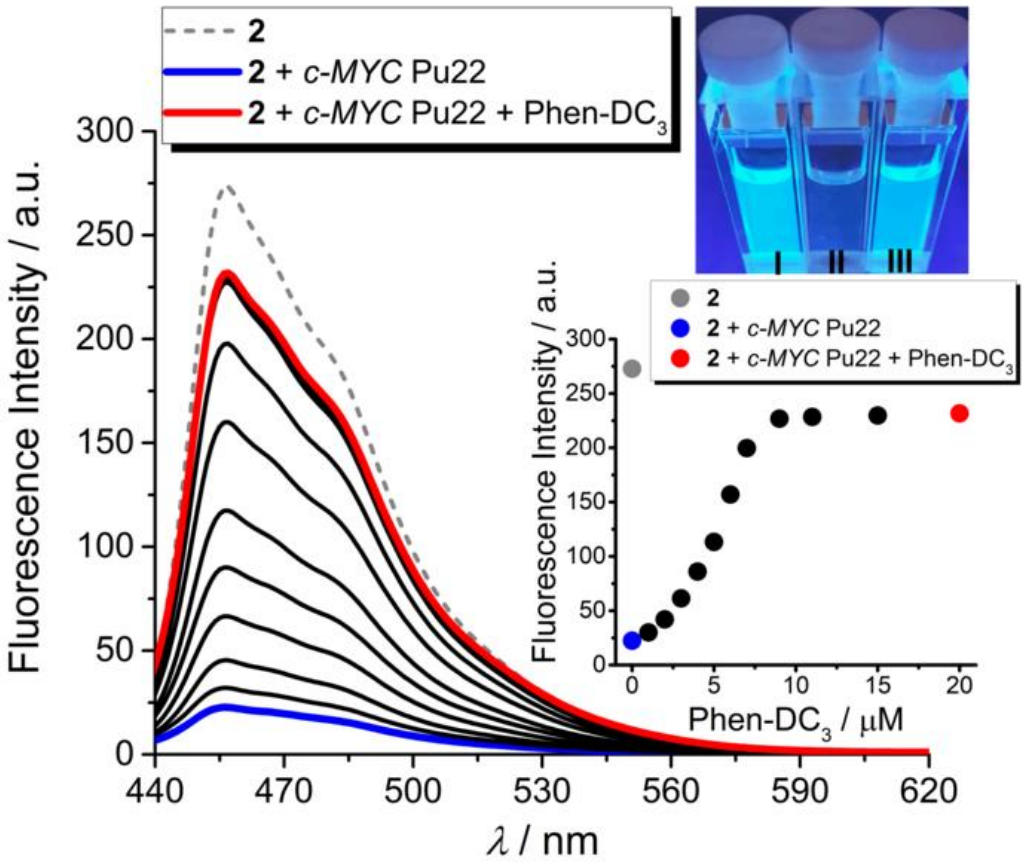

Figure S45 Fluorescence displacement assay performed by using the G4 end-stacker Phen-DC_3. **2** is emissive in its free state (dashed gray line). Complexation with *c–MYC* Pu22 induced fluorescence quenching of **2** (solid blue line). Displacement of **2** from the G4 template by Phen-DC_3 restored the emissive properties of **2** (solid red line). Inset upper panel: Naked-eye detection of **2** before (I: bluish cuvette) and after (II: colorless cuvette) the addition of *c-MYC* Pu22, as well as in the presence of *c-MYC* Pu22 and Phen-DC_3 (III: bluish cuvette) under 312 nm UV light exposure. Inset lower-panel: Fluorescence emission changes at λ_{em} on the **2**-*c-MYC* Pu22 system upon increasing concentration of Phen-DC_3. Experimental conditions: (C_2 = 4.0 μM, $C_{c\text{-}MYC\ Pu22}$ = 4.0 μM, $C_{Phen\text{-}DC3}$ = 0 to 20 μM, C_{KCl} = 100 mM, C_{Tris} = 50 mM pH 7.4, λ_{exc} = 328 nm).

ECD-based thermal melting assay

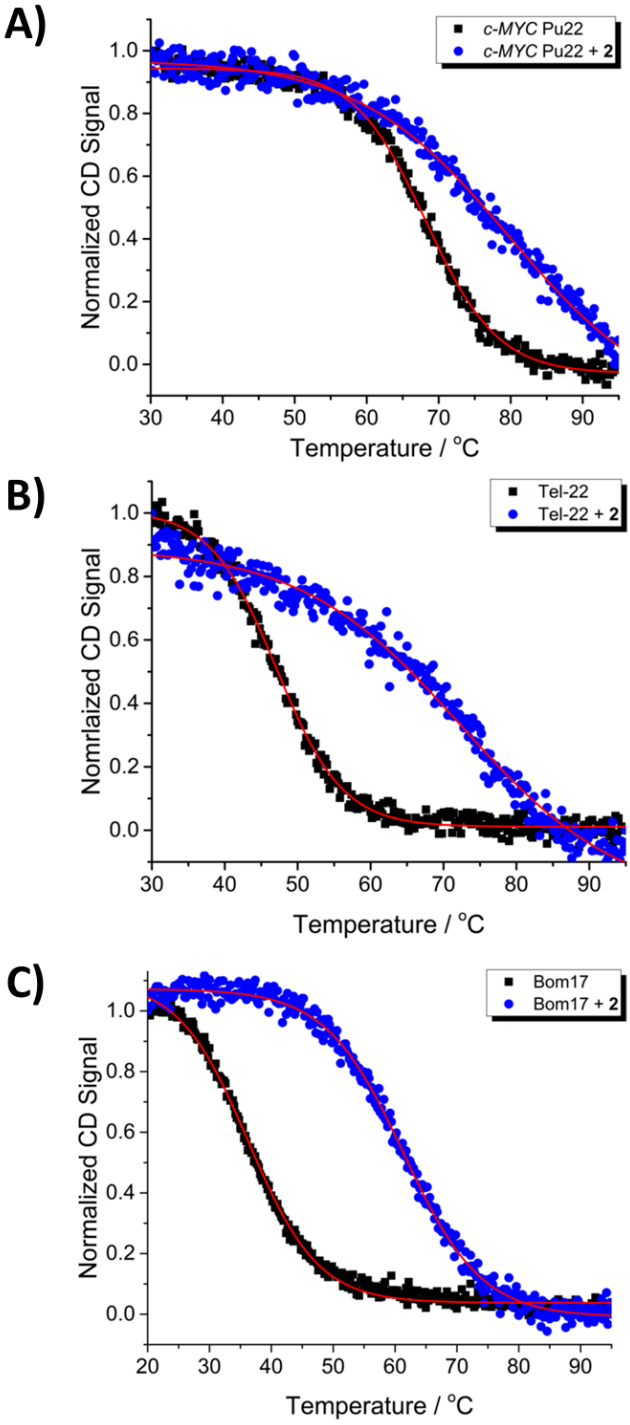

Figure S46 ECD-based thermal melting assay of **A)** *c-MYC* Pu22 (C_2 = 8.0 µM, C_{G4s} = 2.0 µM, C_{KCl} = 5 mM, C_{Tris} = 10 mM pH 7.4), **B)** Tel-22 (C_2 = 8.0 µM, C_{G4s} = 2.0 µM, C_{KCl} = 5 mM, C_{Tris} = 10 mM pH 7.4) and **C)** Bom17 (C_2 = 8.0 µM, C_{G4s} = 2.0 µM, C_{KCl} = 15 mM, C_{Tris} = 10 mM pH 7.4) in the presence of **2**.

Illustration of the Taq-DNA-polymerase stop assay

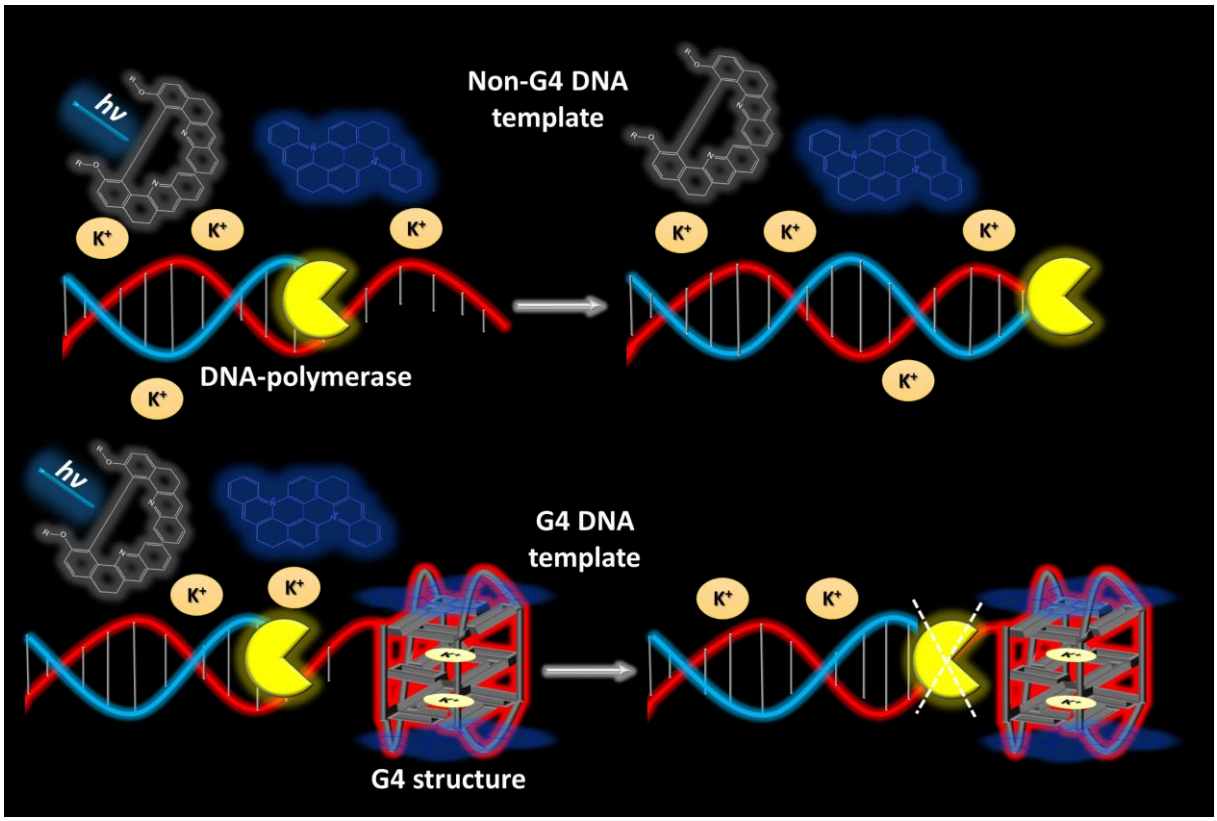

Figure S47 Schematic representation of the light-activated G4 stabilization process mediated by the photoconversion of **1** into **2**. **1** is unable to impact DNA synthesis in both non-G4 and G4-forming sequences. On the other hand, photoconversion of **1** into **2** induced a selective stabilizing effect on the DNA templates containing only the G4 motif, leaving the non-G4 template unaffected.

Taq-DNA-polymerase stop assay with CX-5461

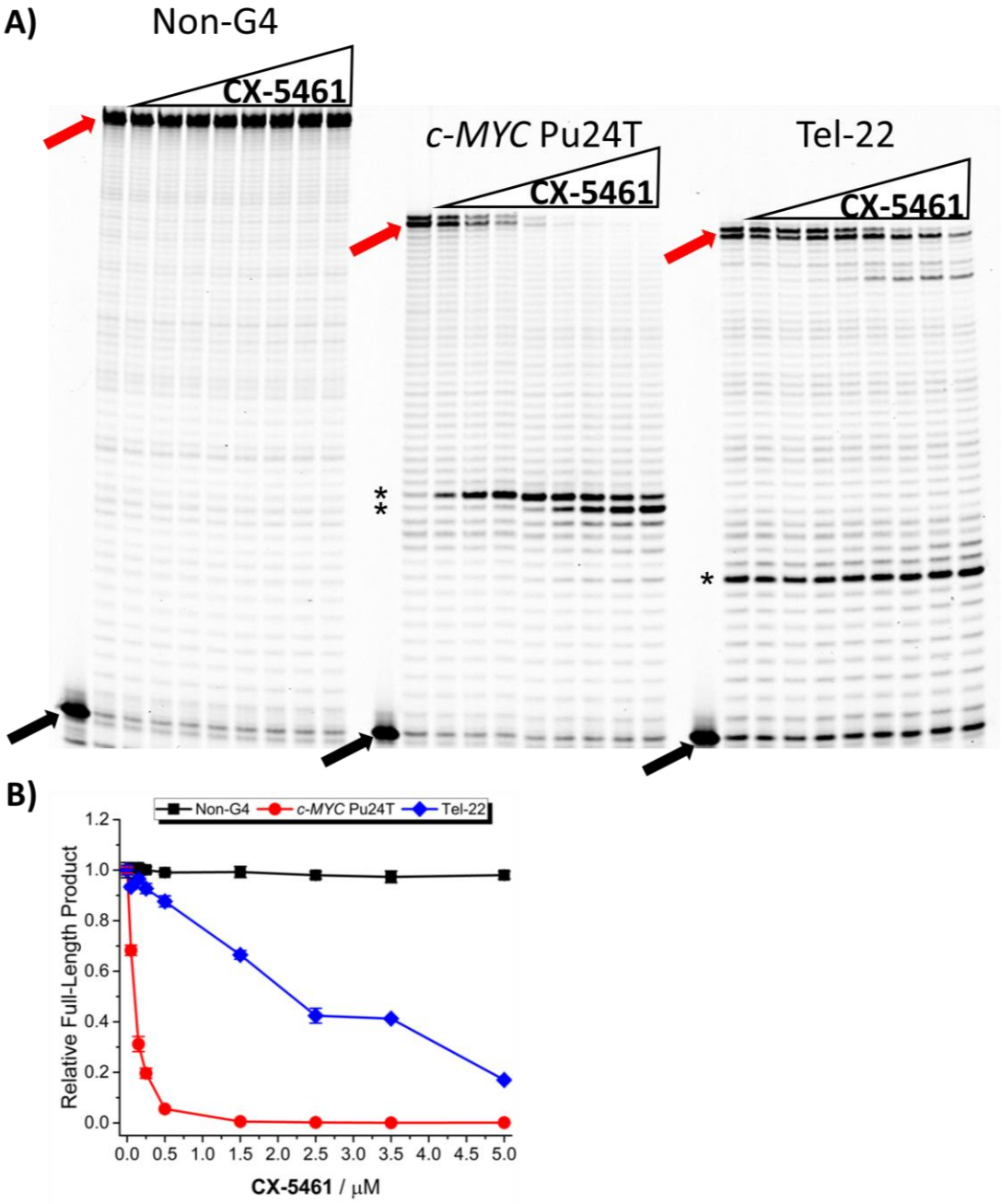

Figure S48 A) Taq-DNA polymerase stop assay with CX-5461. **B)** Relative quantification of full-length products of the gels in (A) normalized to control sample ($C_{CX\text{-}5461}$ = 0 μM). Concentrations of compounds used were ($C_{CX\text{-}5461}$ = 0.0, 0.05, 0.15, 0.25, 0.5, 1.5, 2.5, 3.5 and 5 μM). Black arrows indicate start of the reaction (non-extended primer); red arrows represent full-length products; asterisks represent pausing sites. Error bars represent standard deviations for 3 independent experiments.

In-cellulo photoconversion of compound **1**

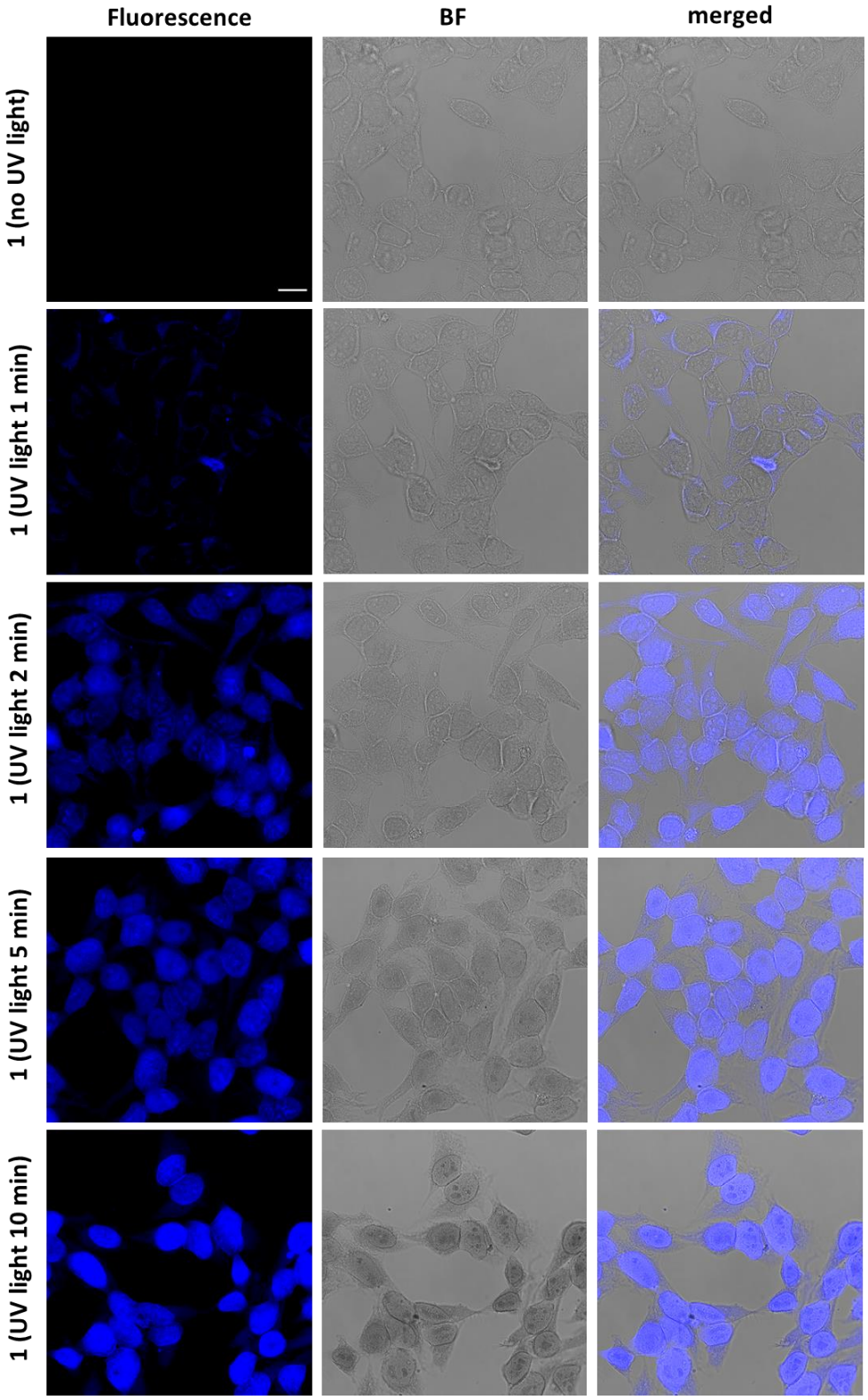

Figure S49 *In-cellulo* photoconversion of compound **1**. Confocal fluorescence images of MeOH-fixed HeLa cells stained with **1** (10 μM) along with the corresponding bright field (BF) and overlay images. The cells were either nonirradiated or irradiated with a 312 nm UV lamp for 1, 2, 5 and 10 minutes. Scale bar = 20 μm. Experimental settings: Diode 405 nm laser was used to image **1** λ_{exc} = 405 nm, λ_{em} 430-630 nm.

Confocal fluorescence images of MeOH-fixed HeLa cells stained with isolated **2** or TMPyP4

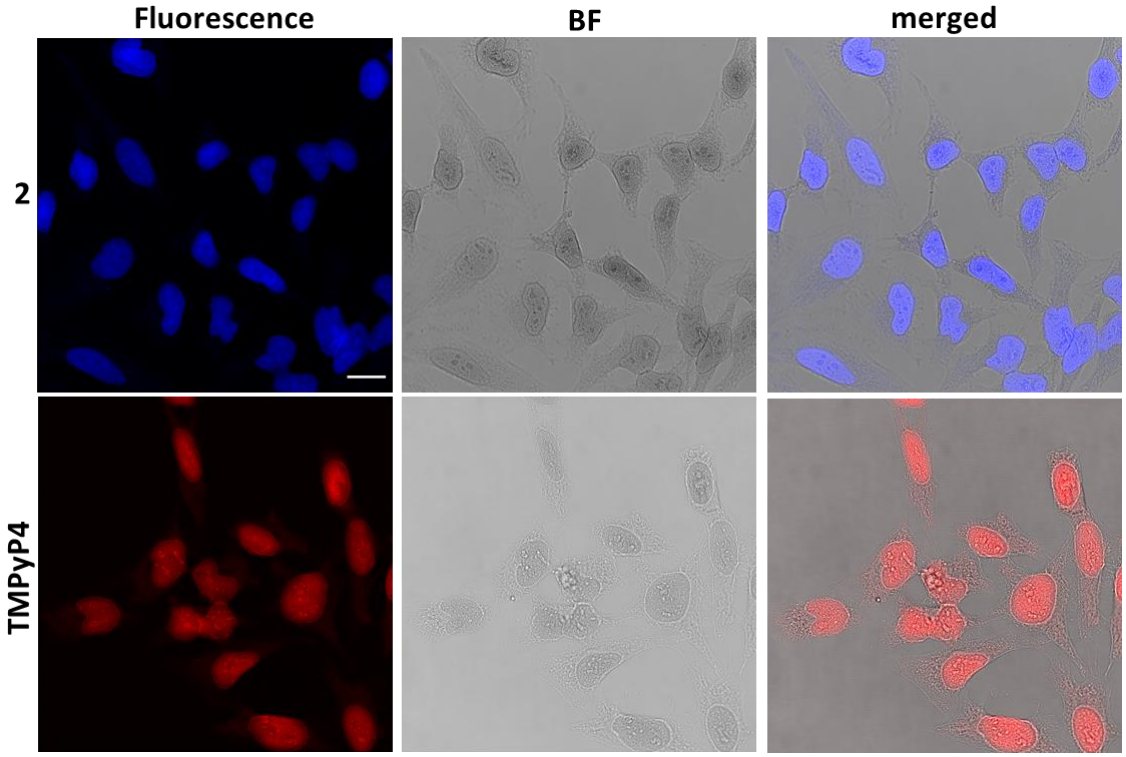

Figure S50 Confocal fluorescence images of MeOH-fixed HeLa cells stained with **2** (10 μM) or TMPyP4 (10 μM) along with the corresponding bright field (BF) and overlay images. Scale bar = 20 μm. Experimental settings: Diode 405 nm laser was used for **2** λ_{exc} = 405 nm, λ_{em} 430-630 nm; Argon laser was used for TMPyP4 visualization λ_{exc} = 514 nm, λ_{em} = 550-700 nm.

Quantitative analysis of the cellular emission fingerprint of 2

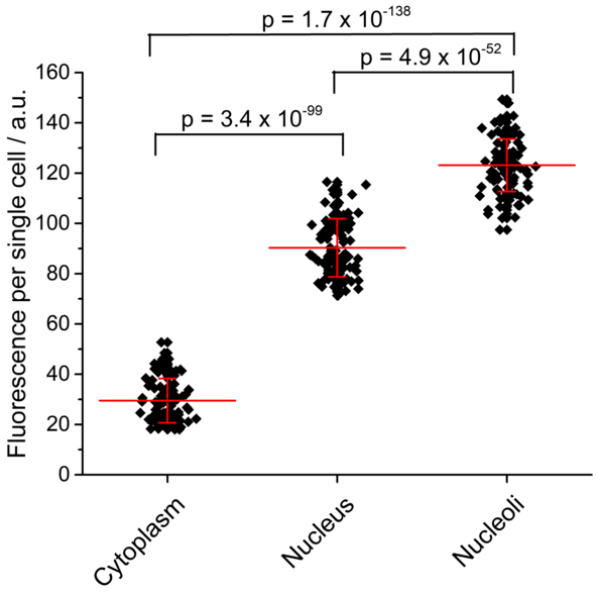

Figure S51 Quantification of fluorescence signal per single cell by selecting the region of interest. Data represent populations of individual cells (N = 100 cells). Means ± SD are indicated. Analysis of the data was performed using two-sample t tests and p values are indicated.

Confocal fluorescence images of RNase treated cells with isolated **2** or Thioflavin T

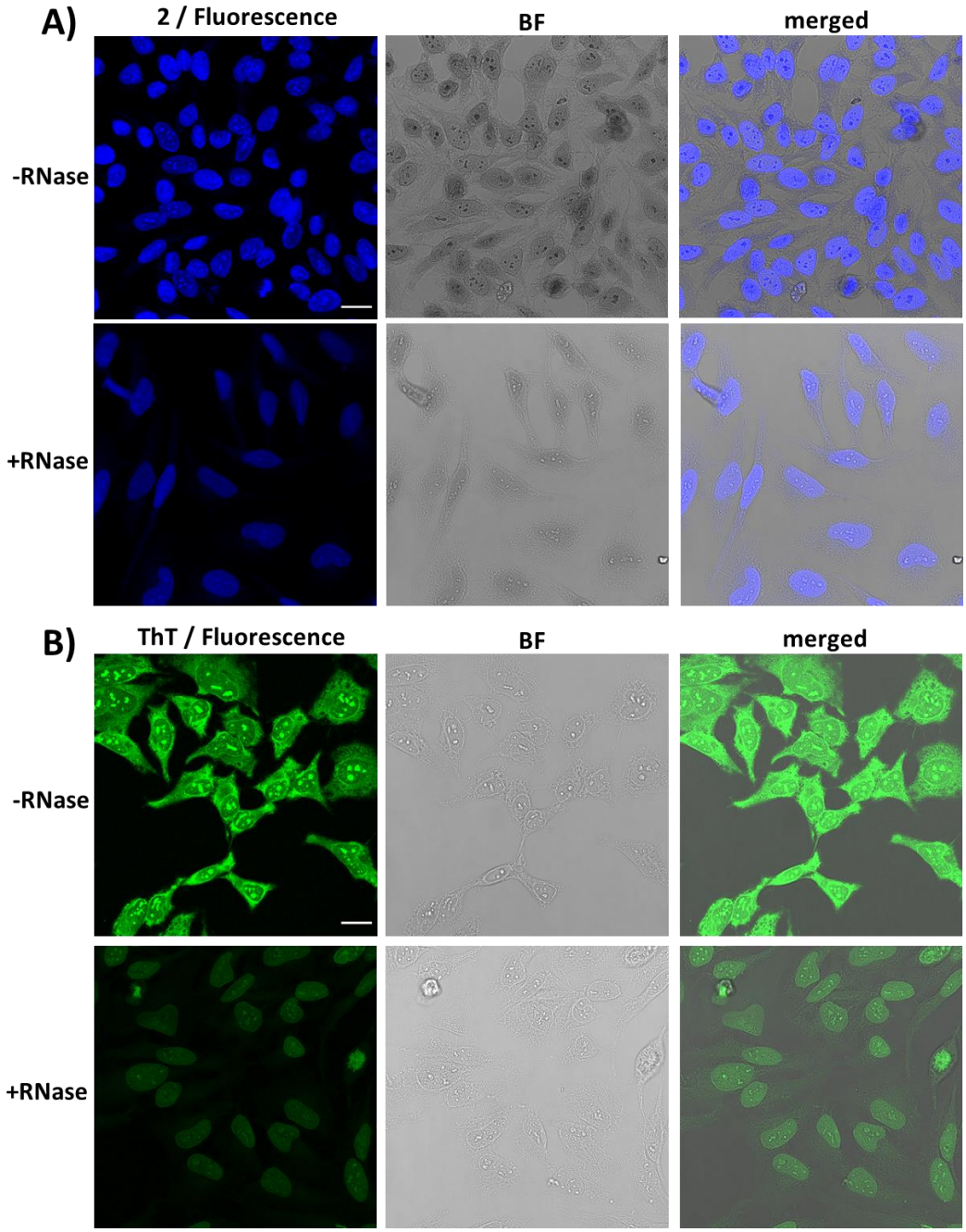

Figure S52 A) Fluorescence images of fixed HeLa cells stained with **2** (10 μM) before and after treatment with RNase. **B)** Fluorescence images of ThT (5 μM) before and after treatment with RNase. Scale bar = 20 μm. Experimental settings: Diode 405 nm laser was used for **2** λ_{exc} = 405 nm, λ_{em} 430-630 nm; Argon laser was used for ThT visualization λ_{exc} = 458 nm, λ_{em} = 480-680 nm.

Fluorescence titration between **2** and RNA G4

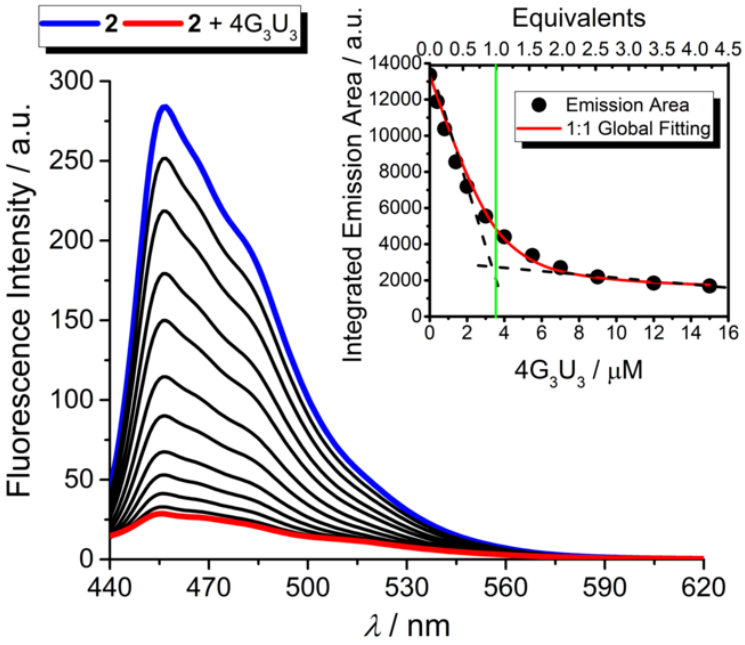

Figure S53 Emission spectra of **2** in the presence of RNA oligonucleotide $4G_3U_3$ (C_2 = 3.6 μM, C_{4G3U3} = 0 to 15 μM, C_{KCl} = 100 mM, C_{Tris} = 50 mM pH 7.4, λ_{exc} = 328 nm). Inset: nonlinear fitting procedure obtained by using a global 1:1 binding model. The dashed black and the vertical green lines indicate the inflection point supporting a 1:1 binding stoichiometry.

ThT-associated fluorescent signal in RNase treated cells

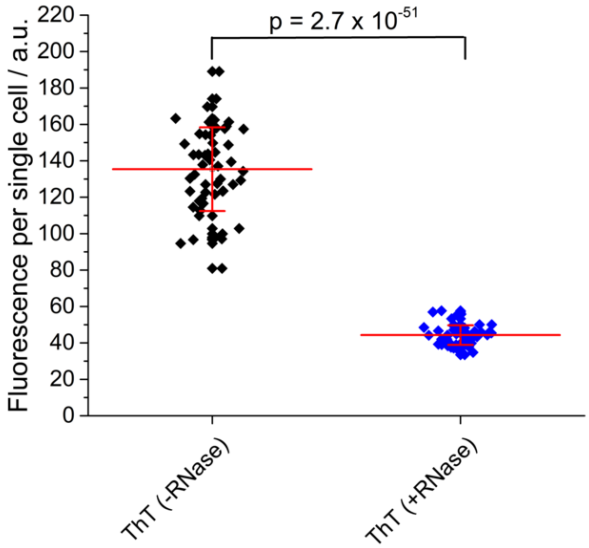

Figure S54 Quantification of fluorescence signal per single cell by selecting the whole cellular area. Data represent populations of individual cells (N = 55 cells). Means ± SD are indicated. Analysis of the data was performed using two-sample t tests and p values are indicated.

Confocal fluorescence images of DNase treated cells with isolated **2** or Hoechst

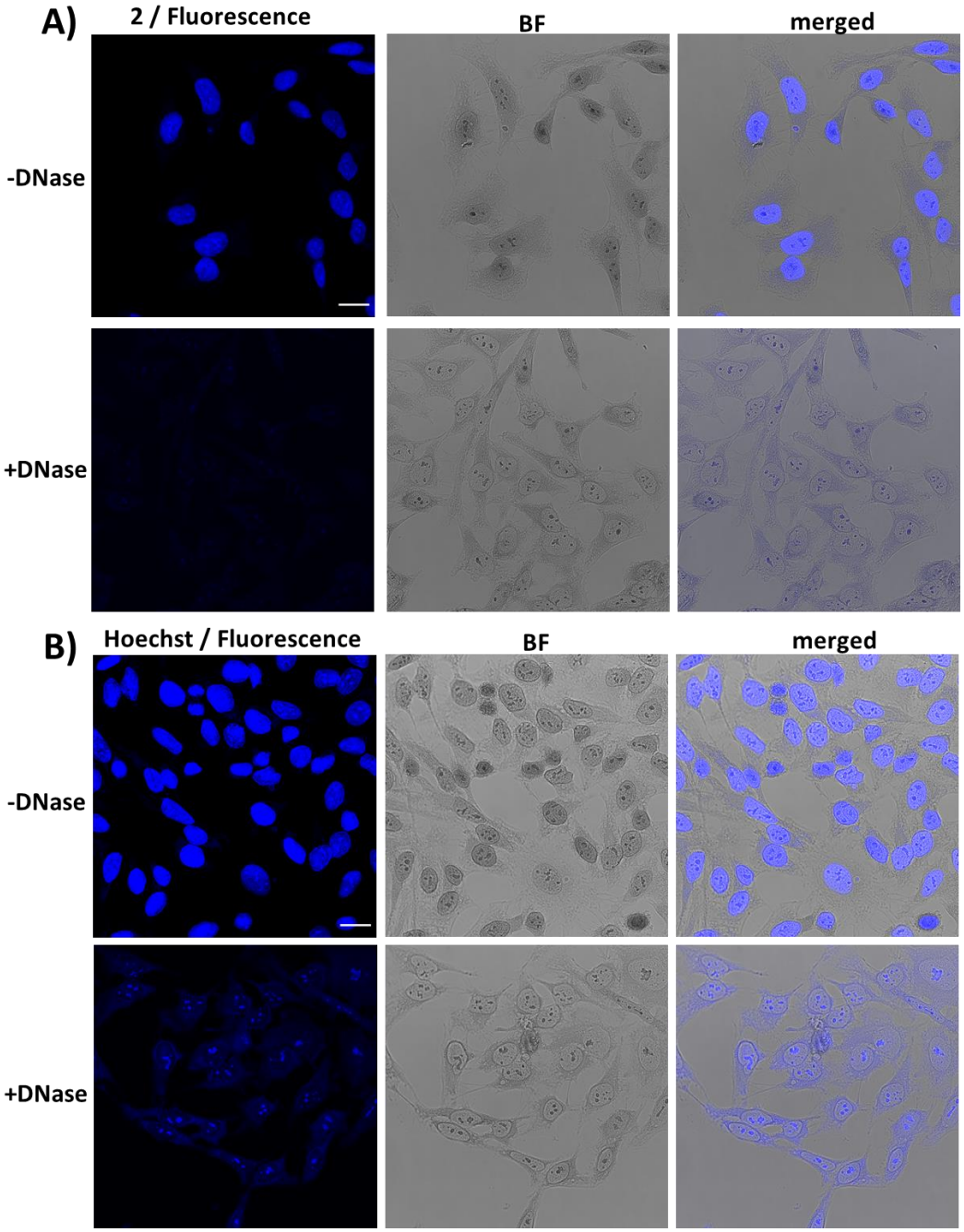

Figure S55 A) Fluorescence images of fixed HeLa cells stained with **2** (10 µM) before and after treatment with DNase. **B)** Fluorescence images of Hoechst 33342 (5 µM) before and after treatment with DNase. Scale bar = 20 µm. Experimental settings: Diode 405 nm laser was used for **2** and Hoechst 33342 λ_{exc} = 405 nm, λ_{em} 430-630 nm for **2** and λ_{em} 430-530 nm for Hoechst 33342.

2-associated fluorescent signal in DNase treated cells

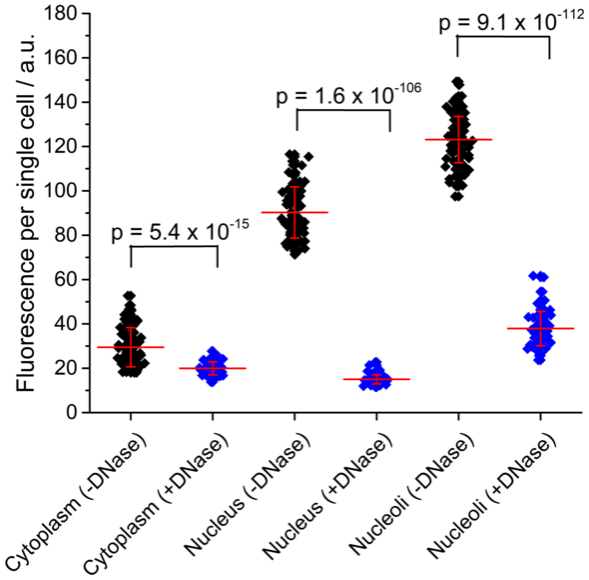

Figure S56 Quantification of fluorescence signal per single cell by selecting the region of interest. Data represent populations of individual cells for each condition of the final experiment: untreated (N = 100 cells) and DNase treated (N = 70 cells). Means ± SD are indicated. Analysis of the data was performed using two-sample t tests and p values are indicated.

In-vitro competition displacement assay between **2** and BRACO-19

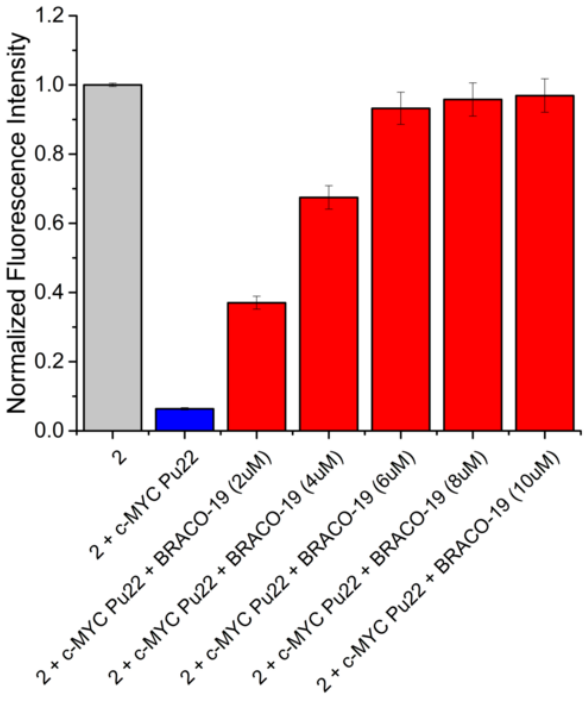

Figure S57 Fluorescence displacement assay performed by using BRACO-19. **2** is emissive in its free state (grey bar). Complexation with *c–MYC* Pu22 induced fluorescence quenching of **2** (blue bar). Displacement of **2** from the G4 template by BRACO-19 restored the emissive properties of **2** in a dose-dependent manner (red bars). The bars represent the fluorescence of **2** at λ_{em}. Experimental conditions: (C_2 = 4.0 µM, $C_{c\text{-}MYC\ Pu22}$ = 4.0 µM, $C_{BRACO\text{-}19}$ = 0 to 10 µM, C_{KCl} = 100 mM, C_{Tris} = 50 mM pH 7.4, λ_{exc} = 328 nm).

Competition binding assay between **2** and BRACO-19

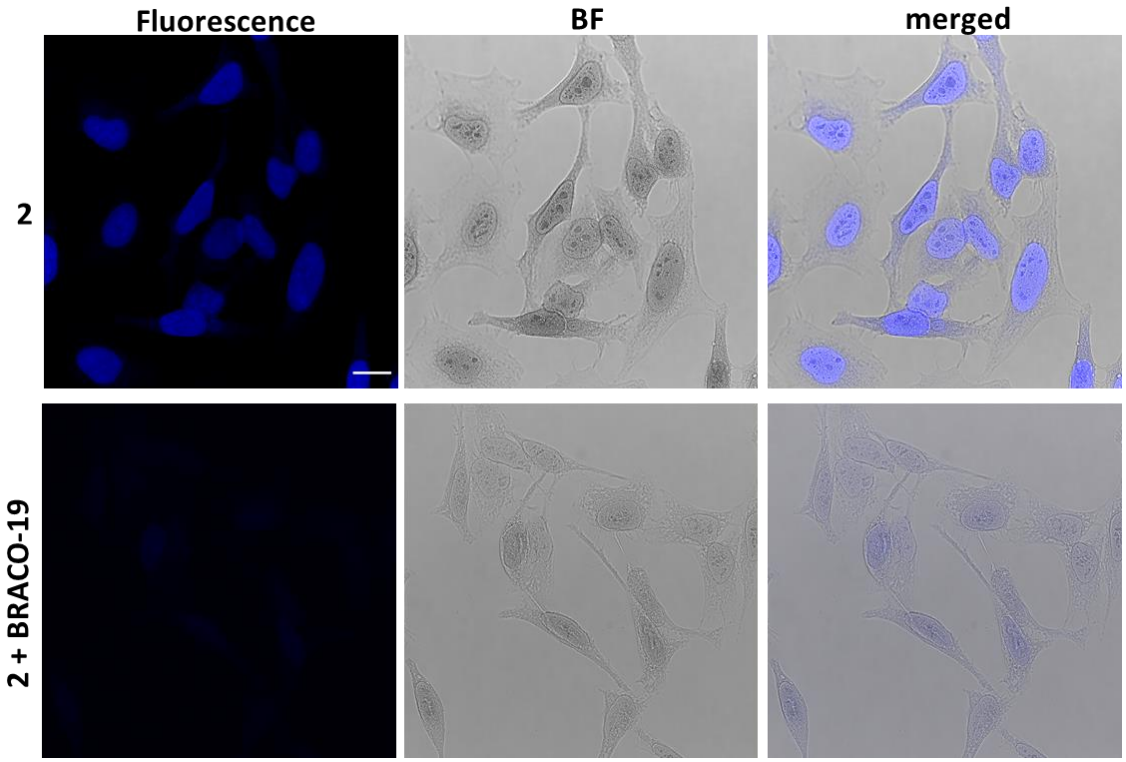

Figure S58 Fluorescence displacement assay between **2** (10 μM) and BRACO-19 (10 μM). Scale bar = 20 μm. Experimental settings: Diode 405 nm laser was used for **2** λ_{exc} = 405 nm, λ_{em} 430-630.

Competition displacement assay between **2** and BRACO-19 in cells

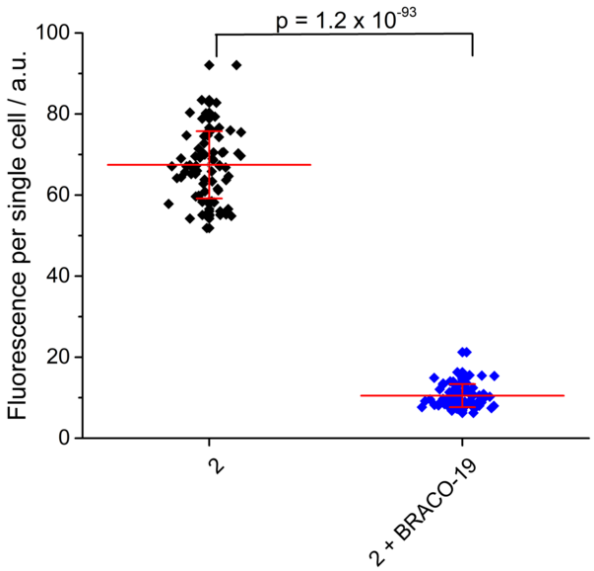

Figure S59 Quantification of fluorescence signal per single cell by selecting the whole cellular area. Data represent populations of individual cells for each condition of the final experiment: untreated (N = 70 cells) and BRACO-19 treated (N = 70 cells). Means ± SD are indicated. Analysis of the data was performed using two-sample t tests and p values are indicated.

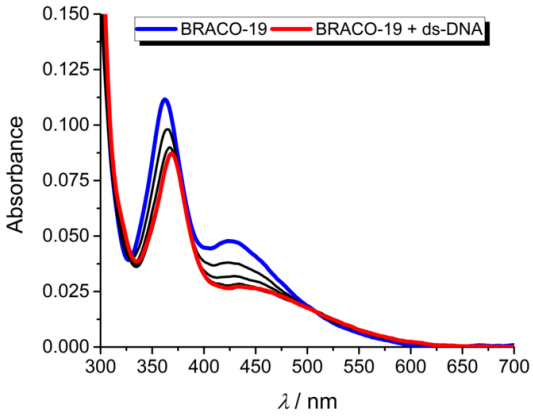

Figure S60 UV/Vis absorption spectra of BRACO-19 (blue line) in the presence of ds-DNA (black and red lines) ($C_{BRACO-19}$ = 5.0 µM, C_{ds-DNA} = 0 to 10 µM, C_{KCl} = 100 mM, C_{Tris} = 50 mM pH 7.4).

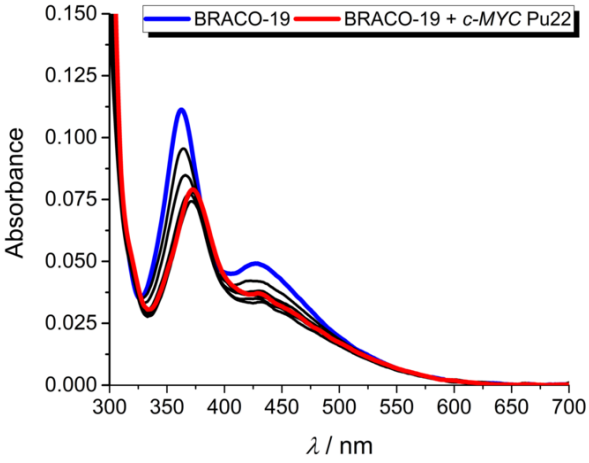

Figure S61 UV/Vis absorption spectra of BRACO-19 (blue line) in the presence of *c-MYC* Pu22 (black and red lines) ($C_{BRACO-19}$ = 5.0 µM, $C_{c\text{-}MYC\ Pu22}$ = 0 to 10 µM, C_{KCl} = 100 mM, C_{Tris} = 50 mM pH 7.4).

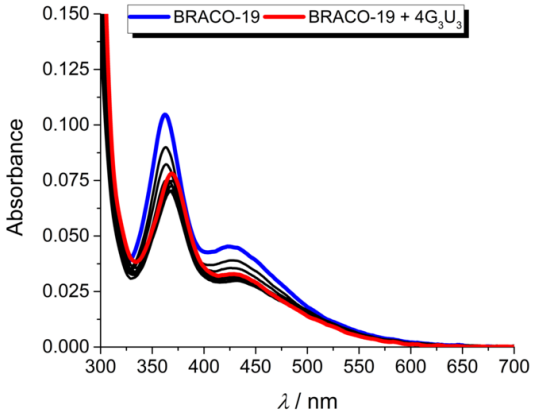

Figure S62 UV/Vis absorption spectra of BRACO-19 (blue line) in the presence of $4G_3U_3$ (black and red lines) ($C_{BRACO-19}$ = 5.0 µM, C_{4G3U3} = 0 to 10 µM, C_{KCl} = 100 mM, C_{Tris} = 50 mM pH 7.4).

Cellular colocalization between 2 and BG4

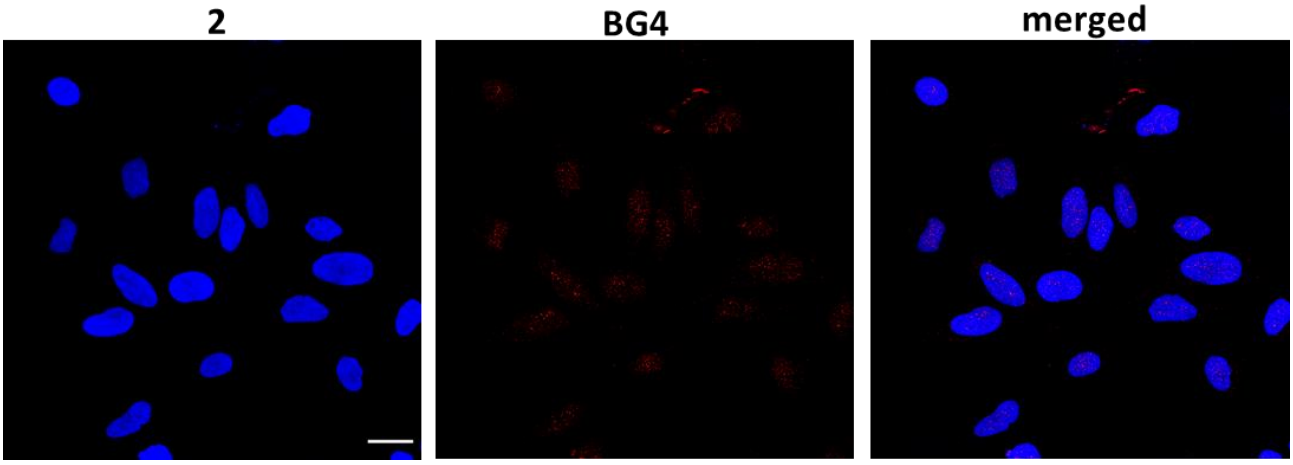

Figure S63 Confocal fluorescence images of PFA-fixed HeLa cells stained with **2** (10 μM) and BG4. Merged fluorescence images demonstrate the nuclear co-localization between **2** and BG4. Scale bar = 20 μm. Experimental settings: Diode 405 nm laser was used for **2** λ_{exc} = 405 nm, λ_{em} 430-480 nm; White light laser (WLL) was used for BG4 λ_{exc} = 598 nm, λ_{em} 620-750 nm.

Molecular dynamics simulations of 2 interacting with ds-DNA, Telomeric and c-MYC Pu22 G4s

All-atom, explicit solvent molecular dynamics simulations were performed to probe the interaction mode of **2** with a ds-DNA sequence, a telomeric G4, and *c-MYC* Pu22, using the Amber 18 suite of programs[9] and the *parm99* force field with bsc1 corrections. A self-complementary 14-bp sequence was built using the Nucleic Acids Builder module of Amber. Telomeric G4 is known to be highly dynamic and able to form a mixture of several G-quadruplexes structures in solution. Therefore, we investigated several human telomeric G4 structures as representative matrices for **2** (see Table S5).

A starting geometry of *c-MYC* Pu22 was taken from the NMR structures (PDB ID code 6O2L) reported by Liu et al.[10] The BMVC ligands were replaced manually by the ligand **2**. Parameters of **2** were generated using the standard procedure implemented with the program antechamber. Atomic partial charges were obtained by the RESP procedure, at the B3LYP/6-31G(d,p) level of theory.

Each system was solvated with TIP3P water molecules with a buffer distance of 14 Å, including potassium and chlorine counterions corresponding to a salt concentration of 0.2 M. The dimensions of the parallelepiped boxes are listed in Table S5.

Table S5 Characteristics of the simulations box for the molecular dynamics of **2** interacting with several DNA and G-quadruplexes systems, as listed in Table S5.

System	PDB	Simulation box	Number of water molecules
ds-DNA d(GTAACGTGTCAATG).(CATTGACACGTTAC)	--	70.4*70.4*84.4	10731
c-MYC Pu22	6O2L	76.4*74.2*75.2	11128
Human telomere repeat d($AG_3[T_2AG_3]_3$) (antiparallel)	143D	67.3*69.6*72.8	9708
Human telomere hybrid-I	2HY9	71.2*69.2*70.1	10693
Human telomere hybrid-II	2JPZ	65.6*71.4*75.7	9954
Human telomere hybrid-III (basket)	2KF8	72.5*76.6*72.2	10339

Minimizations of the solvated structures were performed in 10,000 steps, including 5000 steps of steepest descent. Then a thermalization run was performed for each structure to heat the system from 0K to 300K. The temperature was kept constant during the following steps using Langevin thermostat with a collision frequency γ ln of 1 ps^{-1}. A first 1 ns equilibration run was performed in the NpT ensemble, followed by a second one in the NVT ensemble. Finally, a 200ns production was executed with constant pressure for each system listed in Table S5.

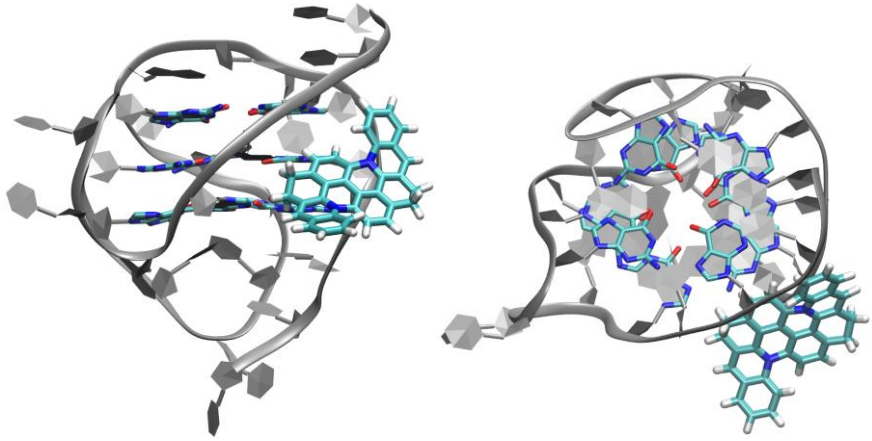

Figure S64 Representative structure for the 1:1 interaction binding mode between **2** and a telomeric G4 model (hybrid-II, PDB ID 2JPZ).

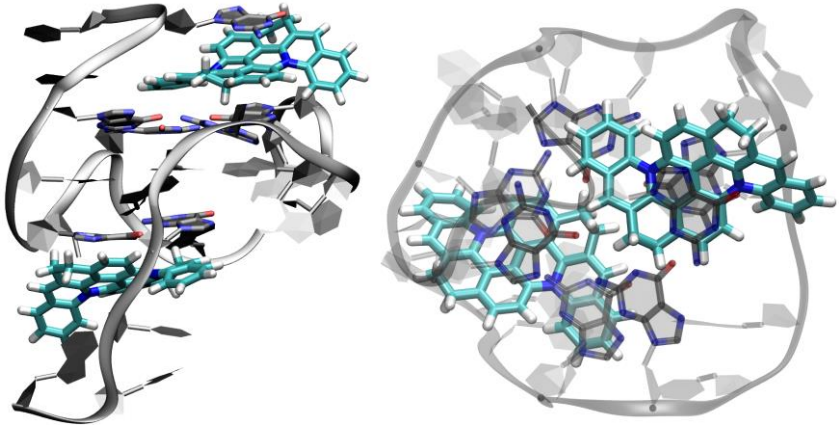

Figure S65 Representative structure for the 2:1 interaction binding mode between **2** and a telomeric G4 model (anti-parallel, PDB ID 143D).

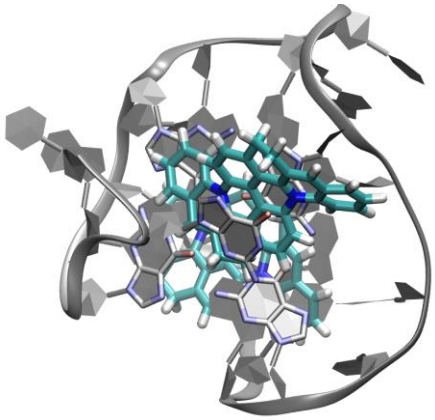

Figure S66 Representative structure for the 2:1 interaction binding mode between **2** and a telomeric G4 model (hybrid-I, PDB ID 2HY9).

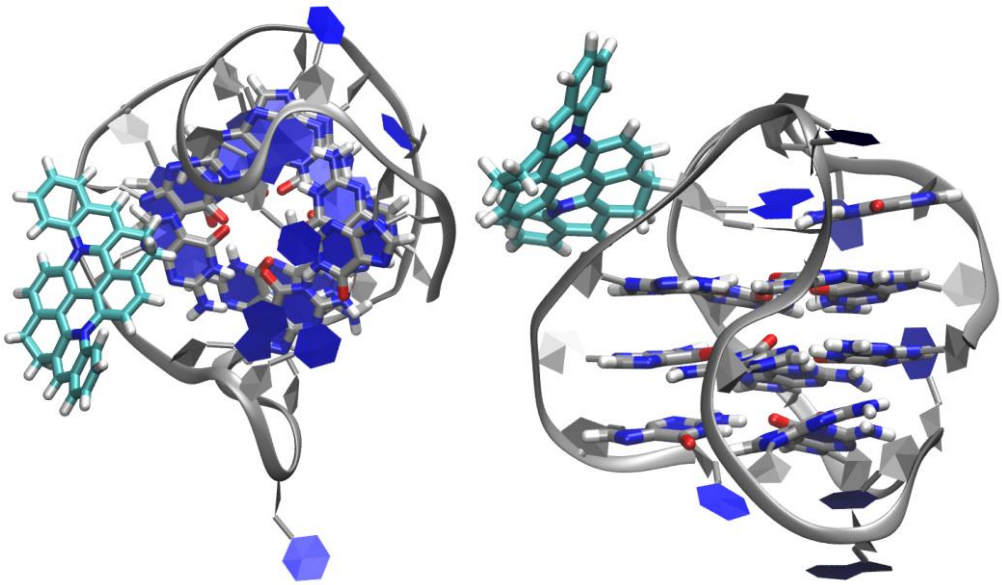

Figure S67 Representative structure for the 1:1 interaction mode (minor groove binding) between **2** and a telomeric G4 model (hybrid III, basket, PDB ID 2KF8).

References

(1) Frisch, M. J., Trucks, G. W., Schlegel, H. B., Scuseria, G. E., Robb, M. A., Cheeseman, J. R., Scalmani, G., Barone, V., Petersson, G. A., Nakatsuji, H. *et al.* Gaussian 16 Revision C.01. 2016.

(2) Adamo, C. and Barone, V. (1999) Toward Reliable Density Functional Methods without Adjustable Parameters: The PBE0 Model. *J. Chem. Phys.*, **110**, 6158–6170.

(3) Jacquemin, D., Wathelet, V., Perpète, E. A. and Adamo, C. (2009) Extensive TD-DFT Benchmark: Singlet-Excited States of Organic Molecules. *J. Chem. Theor. Comput.*, **5** (9), 2420–2435.

(4) Hehre, W. J., Ditchfield, R. and Pople, J. A. (1972) Self—Consistent Molecular Orbital Methods. XII. Further Extensions of Gaussian—Type Basis Sets for Use in Molecular Orbital Studies of Organic Molecules. *J. Chem. Phys.*, **56** (5), 2257.

(5) Hariharan, P. C. and Pople, J. A. (1973) The Influence of Polarization Functions on Molecular Orbital Hydrogenation Energies. *Theor. Chim. Acta*, **28**, 213–222.

(6) Tomasi, J. and Persico, M. (1994) Molecular Interactions in Solution: An Overview of Methods Based on Continuous Distributions of the Solvent. *Chem. Rev.*, **94** (7), 2027–2094.

(7) Aidas, K., Angeli, C., Bak, K. L., Bakken, V., Bast, R., Boman, L., Christiansen, O., Cimiraglia, R., Coriani, S., Dahle, P. *et al.* (2014) The Dalton Quantum Chemistry Program System. *WIREs Comput. Mol. Sci.*, **4** (3), 269–284.

(8) Galland, M., Le Bahers, T., Banyasz, A., Lascoux, N., Duperray, A., Grichine, A., Tripier, R., Guyot, Y., Maynadier, M., Nguyen, C. *et al.* (2019) A "Multi-Heavy-Atom" Approach toward Biphotonic Photosensitizers with Improved Singlet-Oxygen Generation Properties. *Chem. - A Eur. J.*, **25**, 9026–9034.

(9) Case, D. A., Ben-Shalom, I. Y., Brozell, S. R., Cerutti, D. S., Cheatham, III, T. E., Cruzeiro, V. W. D., Darden, T. A., Duke, R. E., Ghoreishi, D., Gilson, M. K., Gohlke, H., Goetz, A. W., Greene, D., Harris, R., Homeyer, N., Huang, Y., Izadi, S., Kovalenko, A., Kurtzman, T., Lee, T. S., LeGrand, S., Li, P., Lin, C., Liu, J., Luchko, T., Luo, R., Mermelstein, D. J., Merz, K. M., Miao, Y., Monard, G., Nguyen, C., Nguyen, H., Omelyan, I., Onufriev, A., Pan, F., Qi, R., Roe, D. R., Roitberg, A., Sagui, C., Schott-Verdugo, S., Shen, J., Simmerling, C. L., Smith, J., Salomon- Ferrer, R., Swails, J., Walker, R. C., Wang, J., Wei, H., Wolf, R. M., Wu, X., Xiao, L., York, D. M. and Kollman, P. A. 2018, AMBER 2018, University of California, San Francisco

(10) Liu, W., Lin, C., Wu, G., Dai, J., Chang, T. -C. and Yang, D. (2019) Structures of 1:1 and 2:1 Complexes of BMVC and MYC Promoter G-Quadruplex Reveal a Mechanism of Ligand Conformation Adjustment for G4-Recognition. *Nucleic Acids Res.*, **47** (22), 11931–11942.